OPTIMIZING THE ION SOURCE FOR POLARIZED PROTONS

SAMANTHA JOHNSON

Thesis presented in fulfillment of the requirements for the degree of Master of Sciences at the University of The Western Cape.

Supervisor: Dr. P. Celliers
Accelerator Group
IThemba Labs

December 2005

DECLARATION

I, the undersigned, hereby declare that the work contained in this thesis is my own original work and that I have not previously in its entirety or in part submitted it at any university for a degree.

Signature: ……

Date: ……

OPTIMIZING THE ION SOURCE FOR POLARIZED PROTONS (ITHEMBA LABS)

SAMANTHA JOHNSON

ITHEMBA LABS, P.O. BOX 722, SOMERSET WEST, 7129

ABSTRACT

Beams of polarized protons play an important part in the study of the spin dependence of the nuclear force by measuring the analyzing power in nuclear reactions. The source at iThemba LABS produces a beam of polarized protons that is pre-accelerated by an injector cyclotron (SPC2) to a energy of 8 MeV before acceleration by the main separated-sector cyclotron to 200 MeV for physics research. The polarized ion source is one of the two external ion sources of SPC2.

Inside the ion source hydrogen molecules are dissociated into atoms in the dissociator and cooled to a temperature of approximately 30 K in the nozzle. The atoms are polarized by a pair of sextupole magnets and the nucleus is polarized by RF transitions between hyperfine levels in hydrogen atoms. The atoms are then ionized by electrons in the ionizer. The source has various sensitive devices, which influence beam intensity and polarization. Nitrogen gas is used to prevent recombination of atoms after dissociation. The amount of nitrogen and the temperature at which it is used plays a very important role in optimizing the beam current. The number of electrons released in the ionizer is influenced by the size and shape of the filament. Optimization of the source will ensure that beams of better quality (a better current and stability) are produced.

The functioning of the different components of the ion source that play a role in the formation of a polarized beam was investigated. Methods for optimizing the source using these different components have been developed. Experiments have been done to test existing methods and components to establish new methods and improving old ones for optimizing the ion source.

TABLE OF CONTENTS

LIST OF FIGURES

CHAPTER 1

MOTIVATION AND OUTLINE

1.1 Introduction

The iThemba Laboratory for Accelerator Based Science (iThemba LABS) is a multi-disciplinary facility and provides beams of energetic charged particles and facilities for basic and applied research. The beams are utilized for isotope production, nuclear physics, biophysics and medical radiation. Radioisotopes are produced for hospitals and industry. The facility runs for twenty-four hours a day, seven days a week. Basic research includes the study of nuclear structures using AFRODITE (AFRican Omnipurpose Detector for Innovative Techniques and Experiments) and nuclear reaction mechanisms using a K600 spectrometer and scattering chamber.

iThemba LABS operates three cyclotrons and a 6 MV Van de Graaff electrostatic accelerator. The large main machine, the separated-sector cyclotron (SSC) is capable of accelerating protons up to 200 MeV and heavier particles up to much higher energies (750 MeV for Xe, for example). Two smaller conventional solid-pole cyclotrons, light-ion injector cyclotron (SPC1) and the second injector cyclotron (SPC2) are used as pre-accelerators for the main machine (SSC). SPC2 can also be used as a backup for SPC1 as an alternate source of protons for therapy**.** Both injectors can accelerate protons to a maximum energy of 8 MeV.

The first injector cyclotron (SPC1) uses an internal Penning Ionization Gauge (PIG) ion source to produce an intense beam of light ions. The proton beam from SCP1 is accelerated to 66 MeV by the main machine (SSC) for radioisotope production and neutron therapy and 200 MeV for proton therapy.

The second injector, SPC2, is designed for heavy ions such as carbon, argon, krypton and other metals and for polarized proton beams. SPC2 uses two external ion sources, the electron cyclotron resonance ion source (ECRIS) and the ion source for polarized ions (SPI) to produce these ion beams. These ion sources are external and need beam lines to transport the ions to the cyclotron. The ECRIS produces beams of heavy ions while the SPI produces a beam of polarized protons. The beams produced in SPC2 could also be injected into the SSC and accelerated to the final energy.

1.2 Motivation for the study

- The purpose of this study is to optimize the source for polarized ions for optimum intensity. The ion source produces a beam of polarized protons which after acceleration through SPC2 has a maximum energy of 8 MeV. Polarized proton beams are accelerated by the SSC to energies ranging from 20 MeV to 200 MeV for research. The SPI is an important tool for the study of spin dependence of the nuclear force by measuring the analyzing power in nuclear reactions. For this purpose beam intensities in the range of 1-20 nA are needed. The intensity of beams produced by the source has to be greatly reduced by the large emmitance of the source. This is especially the case as the beam passes through the inflector inside SPC2. The beam intensity at the exit of the source may be reduced by a factor of 20 when extracted from SPC2. (A factor of 8-10 applies for beams from the ECR ion source because of its smaller emmitance). The aim of this study is to find critical factors that affect the intensity of beams so as to produce a reliable polarized beam of protons with sustainable high intensities of more than 50 μA. This will ensure an extracted beam from the cyclotron of more than 2.5 μA.

- The polarization of the beam is established by the correct tuning of the magnetic fields of the strong and weak field transition units as well as the RF frequencies of these units. The Jachard method is used to determine the starting values of the

magnetic field that are required to measure polarization. This method has the advantage of optimizing the polarization of the beam at the ion source instead of on a target after extraction from SPC2. It therefore avoids the time-consuming process to accelerate the beam through the SPC2 and then try to optimize the polarization. The aim is to obtain these values and to correlate them with the values found when finally measuring the polarization on the target at the nuclear physics experiment.

- A high degree of polarization of protons as well as equal values for the up and down polarization is required for the nuclear experiments.

- The ion source for polarized ions has a number of factors that influence the beam intensity, which can be adjusted to optimize the beam current. These factors are:

    1. The low temperature effect and nitrogen gas.

       By decreasing the temperature of the beam its intensity increases. Although the low temperatures increase the beam current, there is a threshold temperature, below which the beam current decreases. Nevertheless the intensity can be increased again by spraying monatomic nitrogen gas at the entrance of the nozzle. The amount of nitrogen gas used plays an important role in optimizing the beam intensity.

       The relationship between low temperature and nitrogen is one of the most crucial factors in the optimization of the ion source as the beam increases by almost 100% or more. By studying the effects of the low temperature and nitrogen gas in detail, methods of increasing the beam current can be determined, i.e. the correct nitrogen and low temperature relation can be established and used.

    2. RF of the dissociator of the polarized ion source

       The dissociator receives its power from a 13.6 MHz generator. To obtain optimum power at the dissociator an impedance matching box is used to

couple the 50 O power generator to a 50 O load, thus minimizing the reflected power from the dissociator. Knowledge of the range of values of the components (resistance, inductance and capacitance) inside the matching box is valuable to calculate the final values to secure minimum reflected power and therefore more beam intensity. Methods of measuring these values and decreasing the reflected power will be discussed.

3. The beam formation starts in the nozzle and skimmer. The pressure with which the beam enters and leaves the nozzle determines the final beam current. For optimum beam current, the ratio P_e/P_b [Mil88] must be approximately 0.5, where P_e is the exit pressure and P_b is background pressure. The nozzle's shape and size determines the entrance and exit pressure. Designing a nozzle with a correct pressure relation will ensure that the beam intensity is increased.

4. The beam of particles made in the polarized ion source is ionized by electrons from a filament in the ionizer inside the ion source. The filament emits electrons that are accelerated to ionize the beam. The bigger the number of electrons produced, the higher the ionization efficiency (the higher the number of protons produced). To increase the ionization, a filament that produces a bigger number of electrons is needed. The shape and size of the filament influences its resistance and the power that can be delivered by the source. Designing a filament with an optimum resistance will increase the beam intensity.

1.3 Outline of the Thesis

- In chapter two, the cyclotrons operated at iThemba LABS are discussed. The layout of the facilities available at this institution is shown in this chapter.

- The construction, operation of the ion source and the beam formation process is discussed in chapter three. The role that the various components play in beam formation is discussed.

- In chapter four the optimization of the ion source is discussed as well as factors that influence the beam intensity are discussed. Results that were obtained in experiments are displayed in tables and graphs. These results are discussed in detail at the end of each section.

- Nuclear Polarization techniques/ methods and beam depolarization are discussed in chapter five.

- Chapter six contains the conclusions of the entire study in which recommendations are summarized and the importance of the source is discussed. This is followed by a list of references.

CHAPTER 2

LAYOUT OF THE FACILITY

2.1 Introduction

In the late 1960's it became clear that the existing accelerator facilities no longer met the requirements for nuclear physics research. At the same time radiotherapists became interested in accelerators for proton and neutron therapy. This lead to the idea of a multi-disciplinary facility, the National Accelerator Center, in the Western Cape. The name of the facility was later changed to iThemba Laboratory for Accelerator Based Sciences, iThemba LABS. This facility was build within the reach of two major hospitals in this region, Groote Schuur and Tygerberg Hospital, which have major radiotherapy departments.

Facilities at iThemba Labs include: a hospital where a 66 MeV isocentric neutron therapy gantry and a 200 MeV horizontal proton therapy beamline are based, radioisotope production facilities, a K=600 spectrometer, a 1.5m scattering chamber for nuclear physics research and AFRODITE for measuring gamma rays from compound nuclei. The layout of the facility is shown in figure 2.1.

2.2 IThemba Labs Accelerators

The first circular accelerator was developed by an American physicist Ernest O. Lawrence, who won a Nobel Prize for physics in 1939 for a breakthrough in accelerator design. Accelerators are used to accelerate charged particles to high energies. The fast moving particles are used in physics research, radioisotope production and radiotherapy. Heavy ions such as: oxygen, chlorine, krypton, xenon and more are also accelerated at iThemba LABS for various purposes.

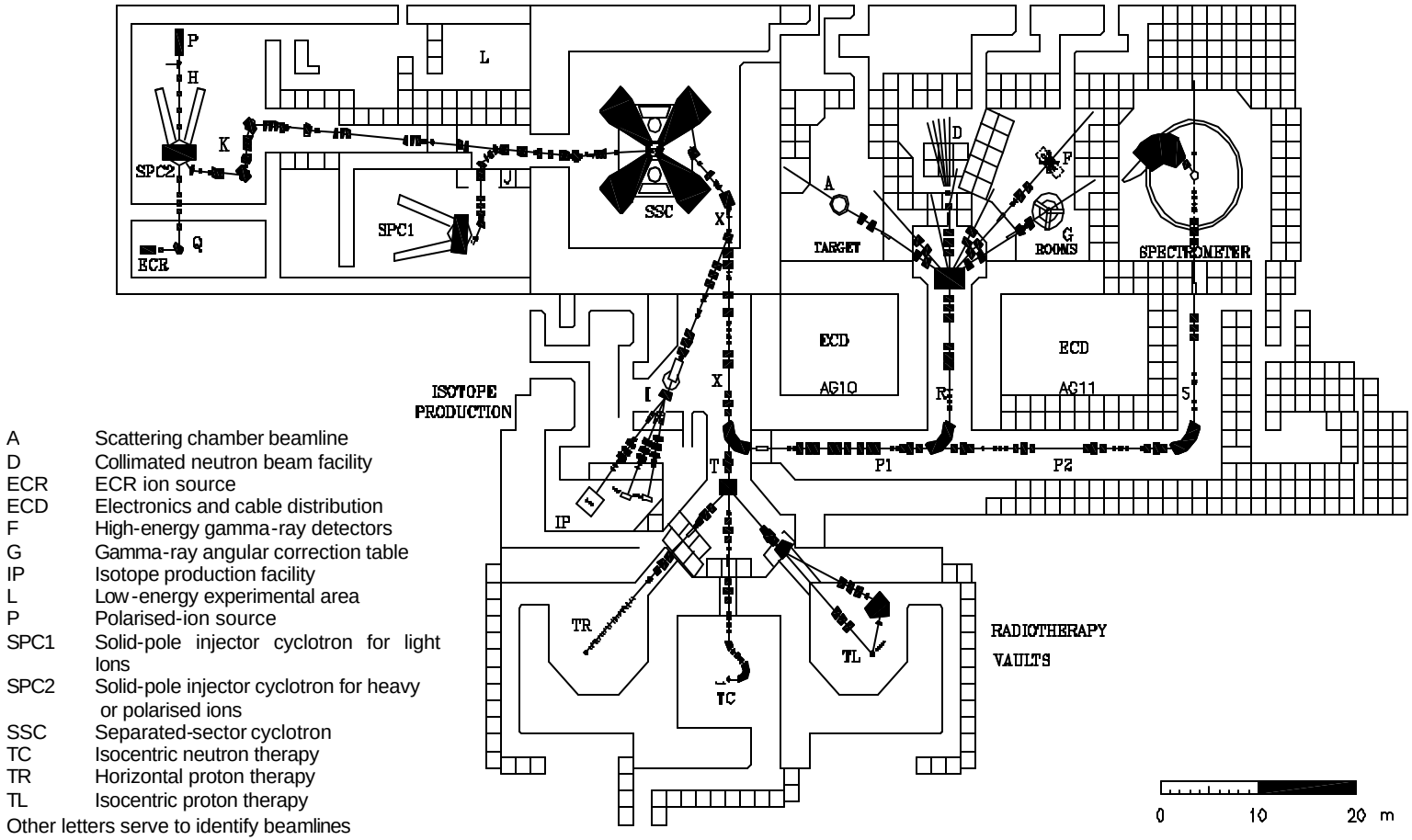

A	Scattering chamber beamline
D	Collimated neutron beam facility
ECR	ECR ion source
ECD	Electronics and cable distribution
F	High-energy gamma-ray detectors
G	Gamma-ray angular correction table
IP	Isotope production facility
L	Low-energy experimental area
P	Polarised-ion source
SPC1	Solid-pole injector cyclotron for light Ions
SPC2	Solid-pole injector cyclotron for heavy or polarised ions
SSC	Separated-sector cyclotron
TC	Isocentric neutron therapy
TR	Horizontal proton therapy
TL	Isocentric proton therapy

Other letters serve to identify beamlines

Figure 2.1: *The layout of the cyclotron facilities at iThemba Labs.*

2.2.1 The separated-sector cyclotron (SSC): K = 200 MeV

The main machine (the SSC) is housed in the main building. The SSC has a diameter of 13.2 m and a height of 7 m. The SSC magnets weights 1400 tons and are positioned to an accuracy of 0.1 mm. The first beam from this cyclotron was extracted in October 1986. The layout of the cyclotron is displayed in figure 2.2. The SSC has four sector magnets with sector angle of 34°. Vacuum chambers are mounted in the pole gaps and between the magnet sectors. The rf system of the SSC consist two $\lambda/2$-resonators which can be tuned over the frequency range of 6 to 26 MHz. The dee voltage produced by an rf power of 100 kW is 250 kV at 26 MHz.

2.2.2 Light- ion solid-pole injector cyclotron (SPC1): K = 8 MeV

SPC1 was the first cyclotron to be constructed and the first beam was extracted in December 1983. This cyclotron uses an internal ion source, a PIG ion source, and pre-accelerates particles to 8 MeV, which are then injected into the SSC. The layout of this cyclotron is shown in figure 2.3. The cyclotron is a four-sector machine with 90° dees and an extraction radius of 0.476 m. The beam is extracted with an electrostatic channel and two magnetic channels. The magnetic field can be adjusted by five trim-coils, two sets of harmonic coils and two cone coils.

2.2.3 The second solid-pole injector cyclotron (SPC2): K=10 MeV

This cyclotron also had four sector magnets with two dees and an extraction radius of 0.476 m. It uses two external ion sources (the ECRIS and SPI) to produce and pre-accelerate heavy ion and polarized proton beams, which are injected axially into it. The layout of SPC2 is shown in figure 2.4. The magnetic field can be adjusted with six trim-coils, two harmonic coils and two cone coils.

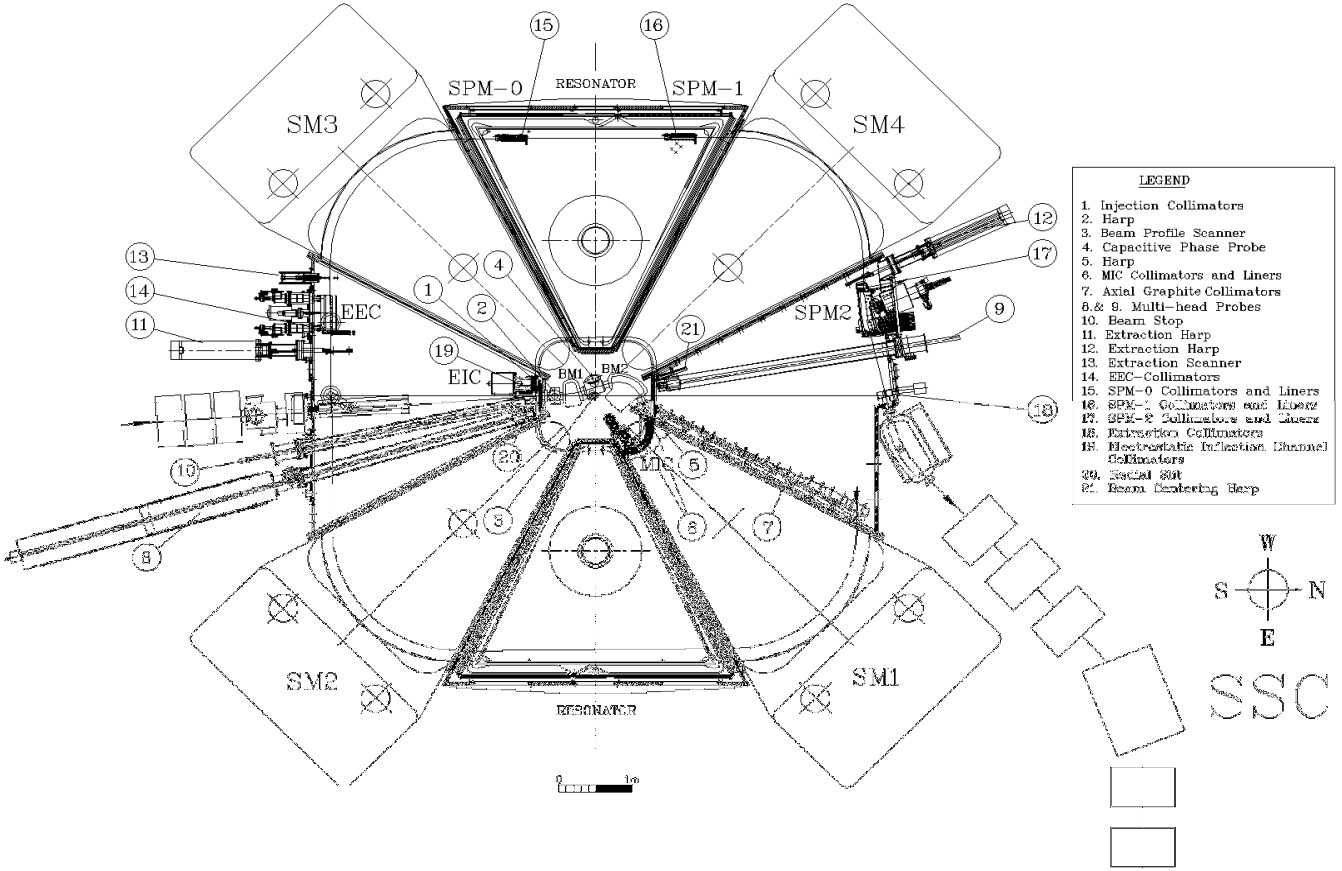

Figure 2.2: *The separated-sector cyclotron (SSC)*

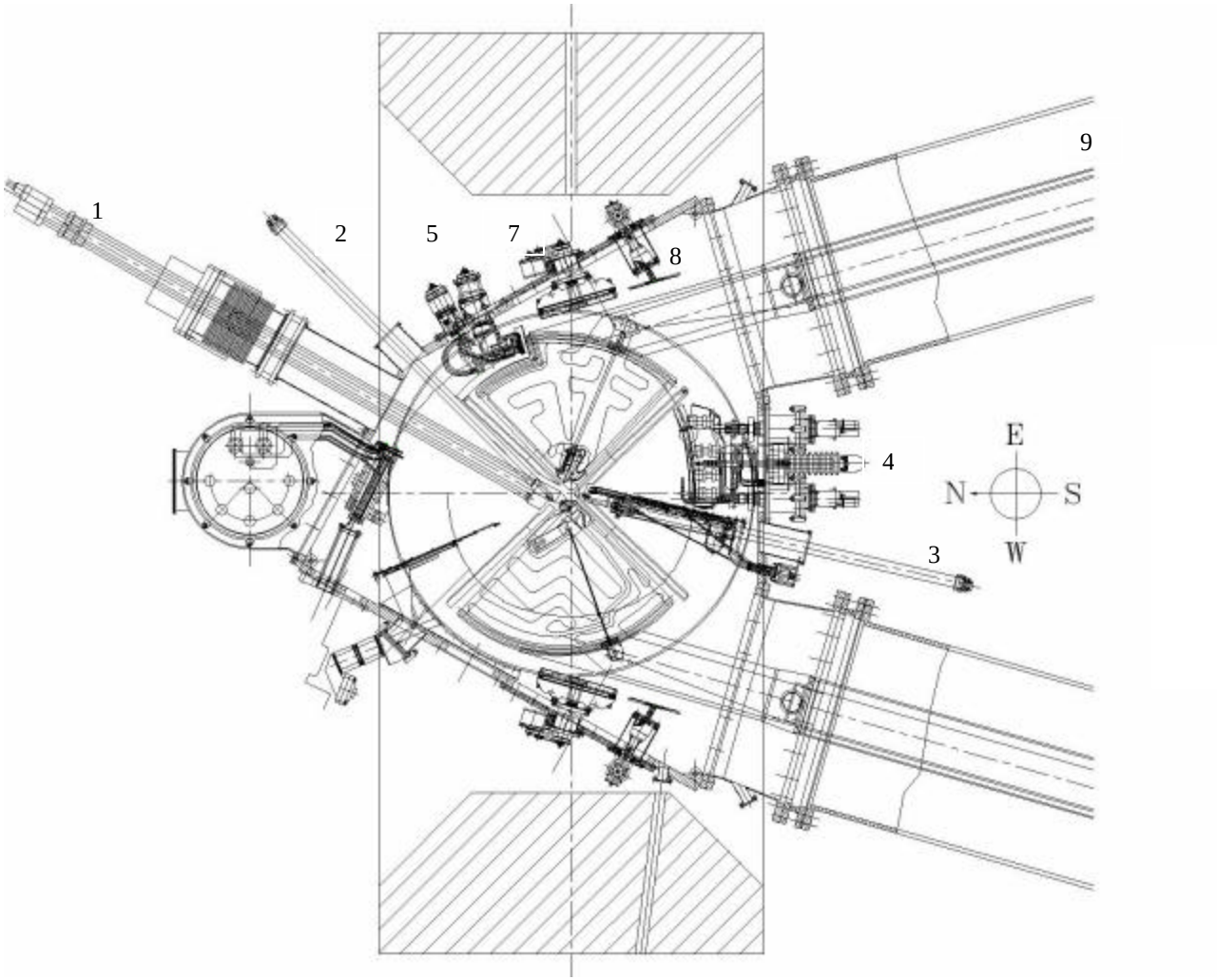

LEGEND

1. Ion Source
2. ΣΔR probe 1
3. ΣΔR probe 2
4. Electrostatic extraction channel (EEC)
5. Magnetic extraction channel 1 (EEC)
6. MEC 2
7. Coupling capacitor
8. Trimming capacitor
9. A resonator

Figure 2.3: *A cross section through SPC1.*

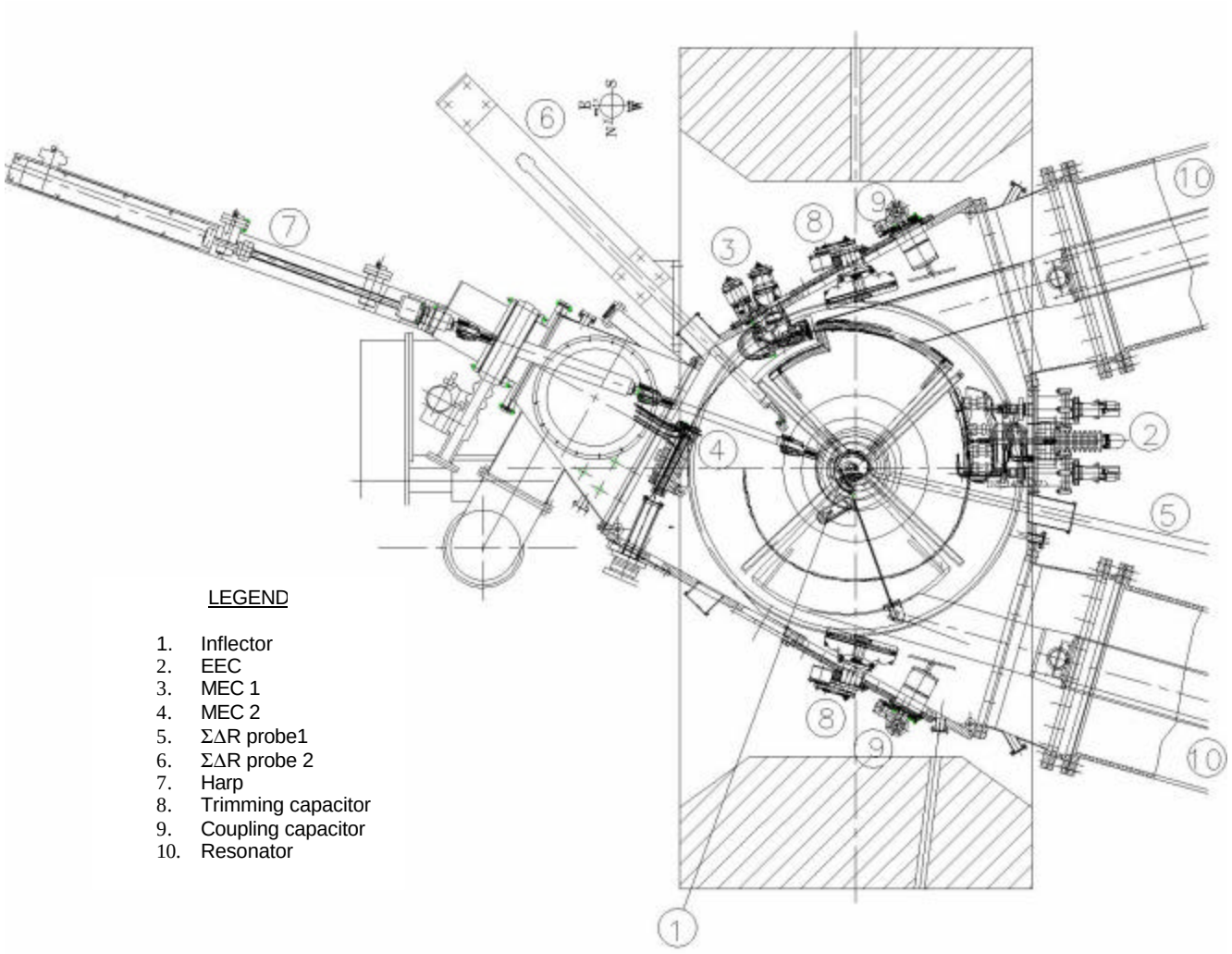

Figure 2.4: *A cross section though SPC2.*

CHAPTER 3

THEORY OF THE POLARIZED ION SOURCE

3.1 Nuclear Polarization

3.1.1 Introduction

There are several ways to obtain nuclear polarized particles. They are:

- The separation of the nuclear spin states by using the Lamb shift,
- The separation of the nuclear spin states by using optical pumping,
- By scattering beams of particles from targets,
- The separation (or quantum mechanical degeneracy of the $1S_{1/2}$ ground state) of nuclear spin states by using inhomogeneous magnetic fields.

The latter process is the one used at iThemba LABS. The separation of nuclear spin states is accomplished by using inhomogeneous magnetic fields and radio frequency induced transitions between occupied and non-occupied levels. The values of the magnetic field and the frequency of the RF transition that is used can be calculated by studying the properties of the fine structured energy levels in hydrogen atoms.

A hydrogen atom consists of a proton and an electron with spin ½. A nucleus in a external magnetic field can have two magnetic spin quantum numbers, $m_I = \pm ½$ corresponding to the alignment of the nucleus that is either parallel or anti parallel to direction of the magnetic field. Polarization of a nucleon beam can be defined as:

$$p = \frac{N\uparrow - N\downarrow}{N\uparrow + N\downarrow}$$

where, $N\uparrow$ and $N\downarrow$ stand for the number of nucleons with parallel and anti-parallel spins relative to the direction of the magnetic field, respectively [Bur63] .

3.1.2 Hyperfine Structure of Energy Levels in Hydrogen

The total angular momentum of the hydrogen atom is composed of the total angular momentum of the electron and the momentum of the proton and is given by:

$$F = I + J \qquad (3.1)$$

J is the angular momentum of the electron and I is the total spin angular momentum of the proton. The possible values of the total angular momentum **F** of the atom can be found by the quantization of the vector **F** and is given by:

$$F = I + J, I + J - 1, \ldots . I - J \qquad (3.2)$$

When J and I are both 1/2, the possible values for F are:

$$F = I + J = 1 \text{ and } F = I - J = 0 \qquad (3.3)$$

The possible values of the magnetic quantum number of the projection of F in the direction of the external magnetic field are given by:

$$m_F = F, F - 1, \ldots, -F + 1, -F \qquad (3.4)$$

The $1S_{1/2}$ state ground state of hydrogen then splits into two hyperfine sublevels (F=0 and F=1). In the presence of an external magnetic field, these different states **F**, will have different energies due to the different orientations of the magnetic dipoles in the external field. The splitting of these energy levels is called the Zeeman effect. The energy difference of these sublevels is determined by the interaction of the nucleon magnetic moment μ_I and the magnetic field produced by the electron at the center of the nucleus.

The energy separation between the levels with F=1 and F=0 can be approximated by using Bethe's equation:

$$\Delta E_{hf} = (\frac{m}{M}) a^4 mc^2 \frac{8g_p}{3n^3}\left[F(F+1) - \frac{3}{2} \right] \qquad (3.5)$$

M (938.27 MeV) and m (0.511MeV) are the proton and electron mass respectively, a the fine structure constant (7.2973×10^{-3}), g_p (2.7928) the proton gyromagnetic ratio, n the principle quantum number and c the velocity of light in vacuum (2.99792×10^{8} ms^{-1}).

In the case of the ground state of the hydrogen atom (n = 1), the energy separation between the states of **F = 1** and **F =** 0 is:

$$\Delta E_{hf} = (\frac{m}{M}) a^4 mc^2 \frac{8g_p}{3n^3}$$

$$\Delta E_{hf}(F=1) - \Delta E_{hf}(F=0) = 5.9\times10^{-6}\, eV$$

The photon corresponding to the transition between these two states has frequency and wavelength :

$$n = 1420.405\, MHz \ and \ \ l = 21.1 cm$$

In the presence of an external magnetic field (H_0) the energy levels split into four substates. These states are called Zeeman hyperfine levels.

Figure 3.1 shows the energy level diagram for hydrogen (J=1/2 and I=1/2) as a function of the magnetic field.

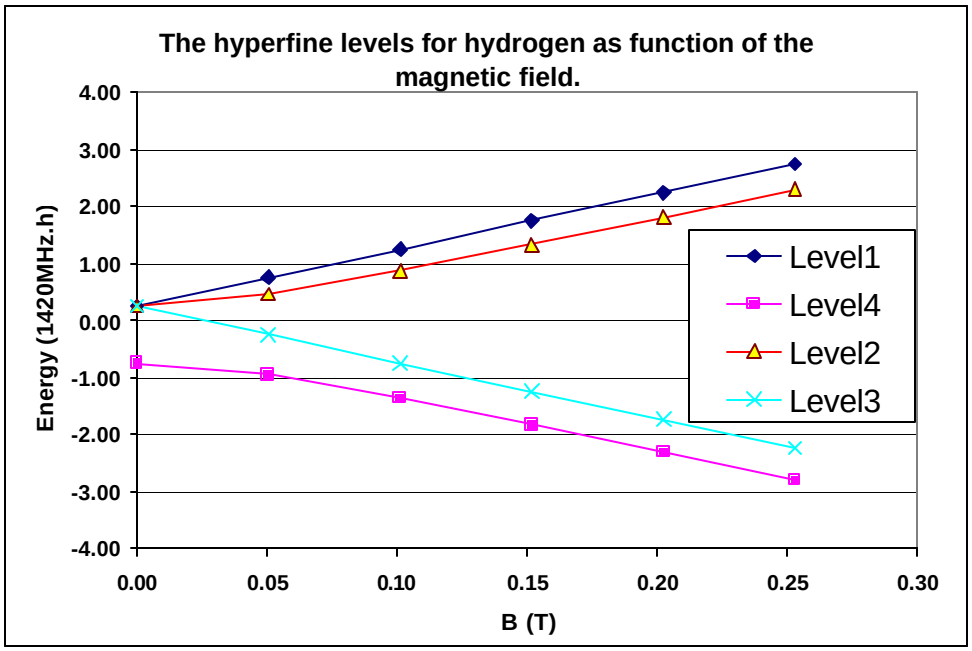

Figure 3.1: *Breit-Rabi diagram of hydrogen showing the behavior of the magnetic substates inside a magnetic field.*

Three levels arise from $m_{f=1}$ namely 1, 0, -1 and one level from $m_{f=0} = 0$ giving a total of four levels and four quantum numbers. Table 3A shows how the levels can be determined.

Table 3A: ENERGY LEVELS

F	LEVEL	m_F	m_I	m_J
1	*1*	*1*	*1/2*	*1/2*
	2	*0*	*-1/2*	*1/2*
	3	*-1*	*-1/2*	*-1/2*
0	*4*	*0*	*1/2*	*-1/2*

m_F is the sum of the projection of I (m_I) and J (m_J) in the direction of the external field. The energy of the sublevels are caused by the interactions between the nuclear moment μ_I and the magnetic field generated by the electron and the spin-orbit, between the electron

and external field H_0 as well as between the nucleus and external field and can be written as the hamiltonian:

$$\mathrm{H} = -m_I H(0) - m_J H_0 - m_I H_0$$

The solution for this hamiltonian is:

$$E_{Fm} = -\frac{\Delta E_f}{2(2I+1)} - m_I H_0 \frac{m}{I} \pm \frac{\Delta E_f}{2}\sqrt{1+\frac{4m}{2I+1}x+x^2} \qquad (3.6)$$

where,

$$x = -(\frac{m_I}{I} - \frac{m_J}{J})\frac{H_0}{\Delta E_f} \qquad (3.7)$$

3.1.3 Construction of the ion source

The ion source for polarized protons was built by a commercial company, Neue Technologien Gmbh, in Germany for research purposes. The construction of the ion source began in 1987. After the completion of the vacuum system and its assembly, it was transported to Forschungzentrum Karlsruhe in 1988. The first beam was made in 1989, which was followed by several adaptations to improve the beam current. At the end of 1989 the ion source was transported back to NTG for further optimization. During this time a staff member of iThemba labs, which was known as the National Accelerator Centre then, was trained to operate the ion source. In August 1990 the source was transported to South Africa, where it arrived at the end of November. The first beam was made soon after the arrival. A photo of the ion source is displayed in figure 3.2 and figure 3.3 depicts a schematic diagram of the source. All the components that contribute to the final polarized beam are marked (figure 3.3) and their functions will be discussed. Special attention will be given to those components that will be investigated to fulfill the requirements of the thesis.

3.1.4 Operational principles of the ion source

Hydrogen gas enters the ion source at the dissociator (see figure 3.2 and 3.3). The gas is manually controlled by a needle valve and its flow is monitored by a flow meter in standard cm^3/minute. The hydrogen is first dissociated in an RF field inside the pyrex tube (see figure 3.4) of the dissociator that transforms the molecules into an atomic beam. The beam then passes through a cooled nozzle made from copper to produce a low temperature, slow moving beam. The beam then continues through the first vacuum chamber into the 'zone of silence', through the skimmer inside the second vacuum chamber and then passes down the axis of a pair of sextupole magnets. These magnets focus the beam with the atoms in the ½ electron spin state for maximum acceptance in the ionizer and deflect the atoms with the unwanted electron spin.

The electron polarized atom in the $1S_{½}$ state now passes through two RF transition units called the weak field (WF) and strong field (SF) units (figure 3.3). Nuclear polarization is accomplished by choosing the correct RF frequencies and magnetic field to populate specific hyperfine levels inside the atom. Finally, this neutral atomic beam is ionized before it can be injected into SPC2. Ionization is induced by fast electrons (± 1 keV) impacting with the polarized atoms. The electrons are confined to a tantalum column by means of four solenoid coils. The column and all its electrodes (figure 3.11) are held at a high electric potential, the extraction voltage of the source. Finally, the beam is focused by an einzel lens and solenoid magnet. A 100- degree-bending magnet is used to bend the beam onto a faraday cup to measure the beam intensity.

3.2 Atomic beam formation

The polarized proton beam starts as a flux of hydrogen gas that has to go through various stages of refinement until it is useful. The steps and the processes that take place when the beam is formed are listed in the following pages.

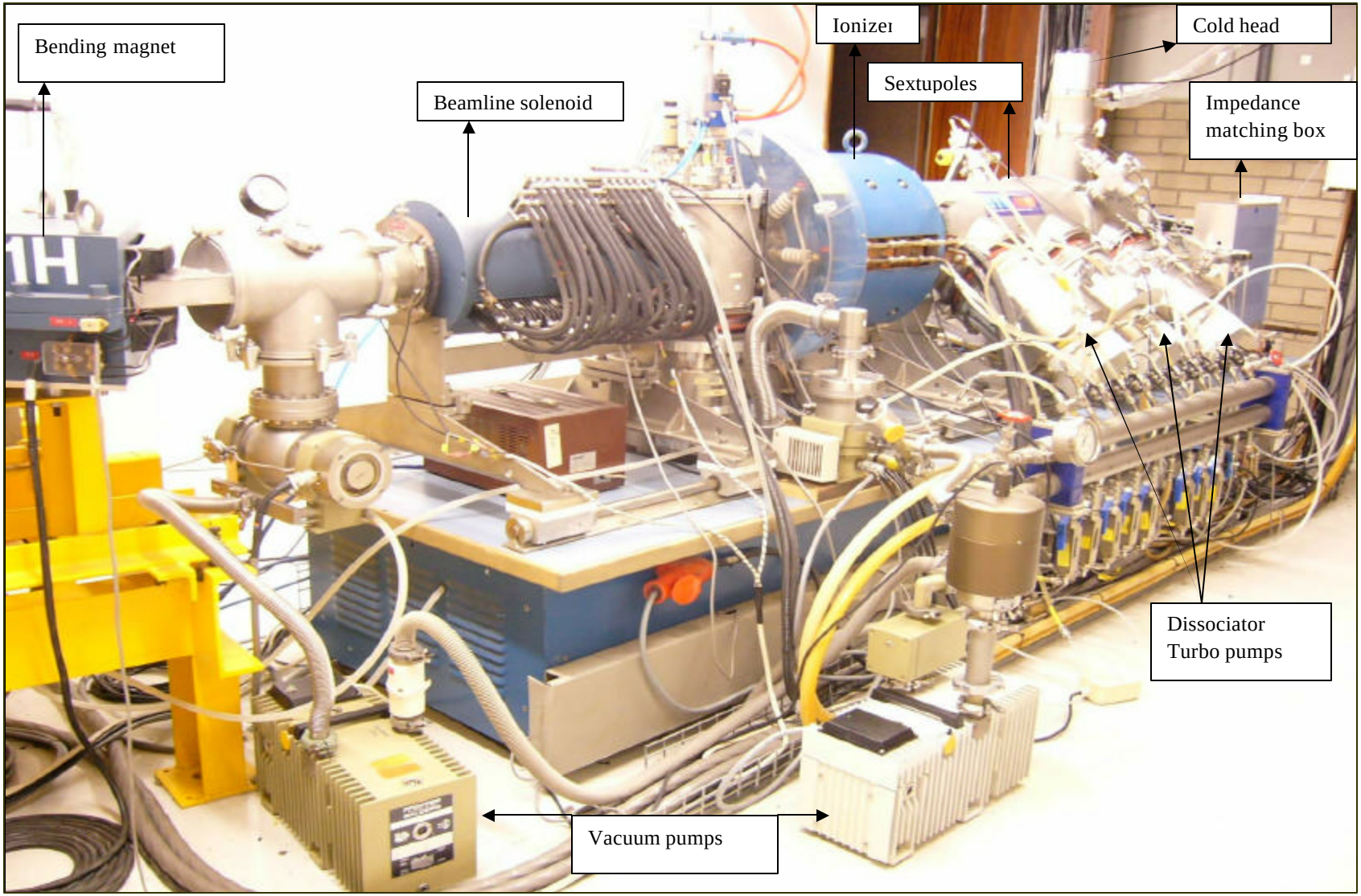

Figure 3.2: *A photo of the ion source for polarized protons at iThemba Labs.*

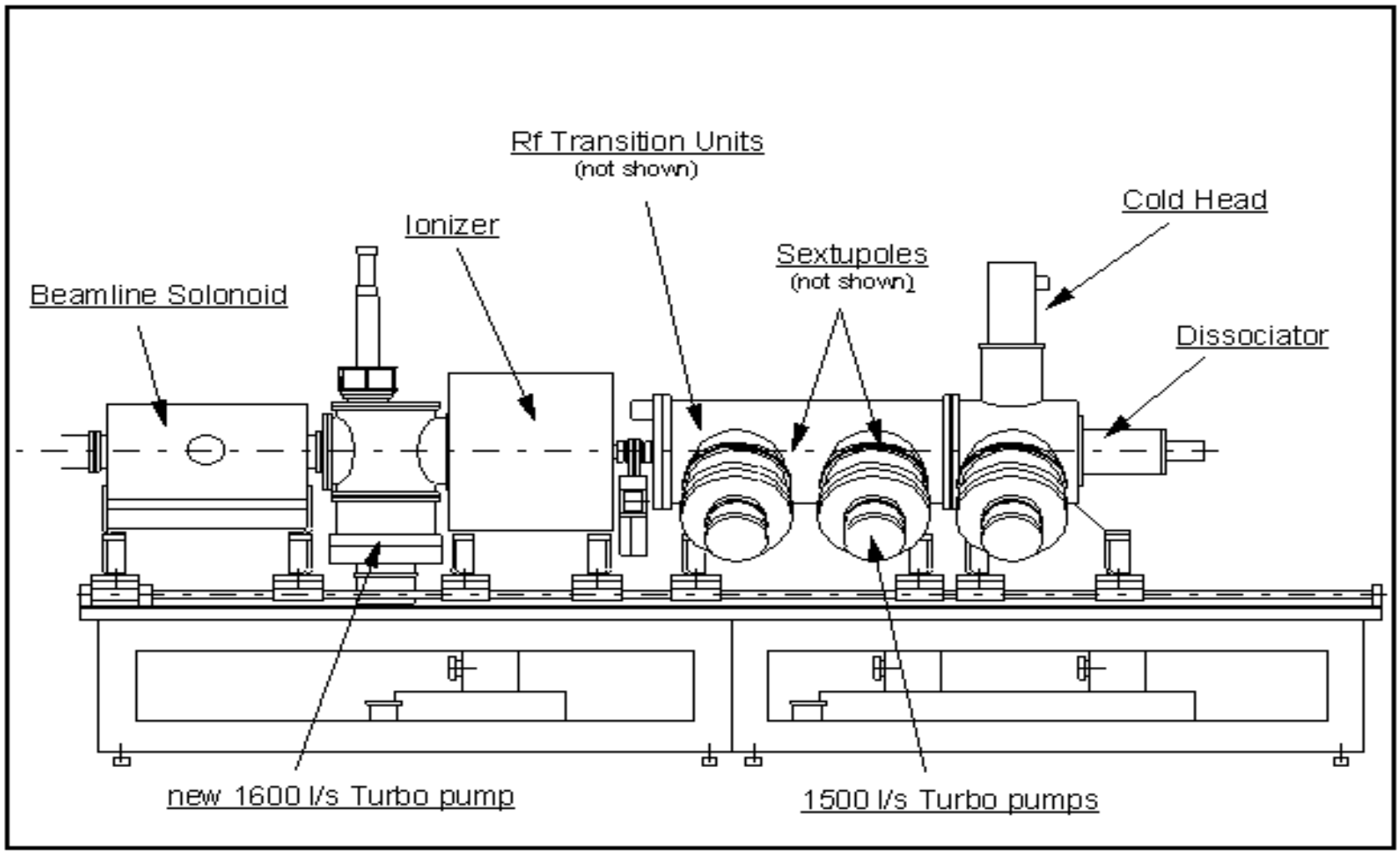

Figure 3.3: *Schematic diagram of the ion source.*

3.2.1 The dissociator

Hydrogen atoms are dissociated in a glass tube inside a copper coil through which a high frequency current is passed. The power dissipated in the coil and the discharge is 175 W or more at a frequency of 13.6 MHz. The power is supplied by a generator with a maximum power of 500 W. The copper coil is part of an LC resonant circuit, which is easily capacitively tuned to 50 ohm through an impedance matching network to minimize the reflected power to the oscillator to practically zero. The dissociation occurs in a 30 cm long glass tube (see figure 3.4) with an inner diameter of 13.5 mm inside the dissociator. The discharge is cooled by water flowing between the dissociator tube and the second tube, with a larger inner diameter that surrounds it. The tube is made of pyrex glass that is very effective in minimizing recombination on its surface. This discharge tube is cooled by water at 20 °C, which is also circulated through the copper coil. The equation for the dissociation is:

$$H_2 + 4.5\ 2eV = 2H + \text{Energy} \qquad (3.8)$$

Figure 3.4 shows the Pyrex tube with the copper coil around it.

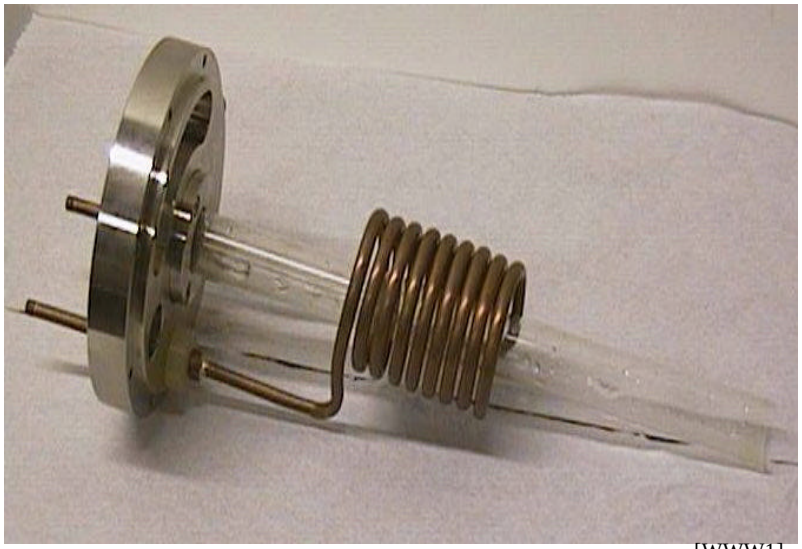

Figure 3.4*: Pyrex tube (glass tube) and copper coil.* [WWW1]

The degree of dissociation is given by:

$$a = \frac{P_1 - P_2}{P_1} \qquad (3.9)$$

where,

P_1 is the atomic flux with the RF on,

P_2 is the atomic flux when the RF is off.

The value of α decreases when recombination increases. Heat is also absorbed on the surface of the glass when recombination takes place. An energy of 4.52 eV is dissipated for each atom being recombined. The intensity of the atomic beam therefore decreases when the intensity of molecules increases. The dissociation degree is influences by the rf power and the flow of hydrogen gas into the ion source (discussed in chapter 4.4).

The discharge in the dissociator glows pink and the colour becomes brighter when the power from the 13.6 MHz generator is increased and the reflected power is minimized and therefore more hydrogen molecules are dissociated into atoms. A poor colour indicates a low atomic content [Dic65]. The amount of light that is produced inside the dissociator resulting from the energy given off by the particles during the dissociation process is measured by a light meter. A value between 80 % and 100 % on the meter is an indication of the effectiveness of the dissociation process. The colour inside the tube is also to some extent an indication of the reflected power from the RF generator although this is measured by a reflectometer. When the reflected power is high the light becomes dim and the light meter reading is usually low (below 60%). For high values of α the light meter readings are also high.

Methods of minimizing the reflected power are discussed in chapter four. The power used for the dissociation process is usually between 100 W and 200 W, depending on the amount of hydrogen gas used and the final beam intensity required. Optimal beam intensities can be produced by correct tuning of the RF power to ensure maximum dissociation (see Chapter 4: rf of the ion source). For higher beam intensities more power

is required to ensure maximum dissociation of molecules into atoms but at a power of more than 200W the intensity reaches a plateau.

3.2.2 Nozzle and Skimmer

The function of the nozzle is to accelerate the atoms passing through it by creating a pressure gradient before the beam escapes into the next vacuum chamber. Schematic diagrams depicting the components connected to the nozzle and the layout are given in figures 3.5 and 3.6. The nozzle is made of oxygen-free, high-conductivity (OFHC) copper or aluminum. The aperture at the end of the tapered nozzle is 3 mm in diameter. The nozzle is cooled to approximately 30 K by a 10 W closed-cycle helium refrigerator and thermally isolated from the discharge tube by a Macor accommodator (shown in figure 3.6). Connection to the refrigerator is made via a heavy, flexible copper braid. Its end is soldered into OFHC copper blocks, which is attached to the refrigerator cold head and the other end tightened around the nozzle. The entire 30 K refrigerator-nozzle assembly is then wrapped with several layers of aluminized mylar for thermal insulation.

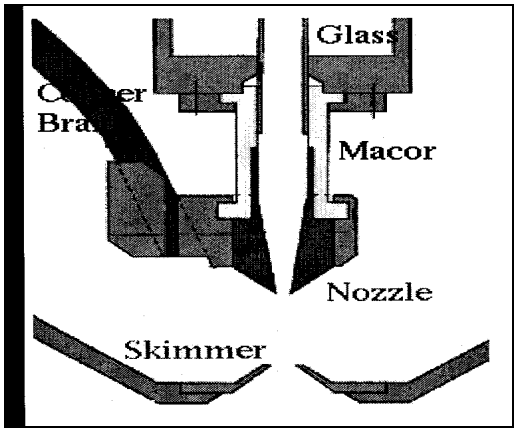

Figure 3.5: *The nozzle and skimmer.* **[WWW2]**

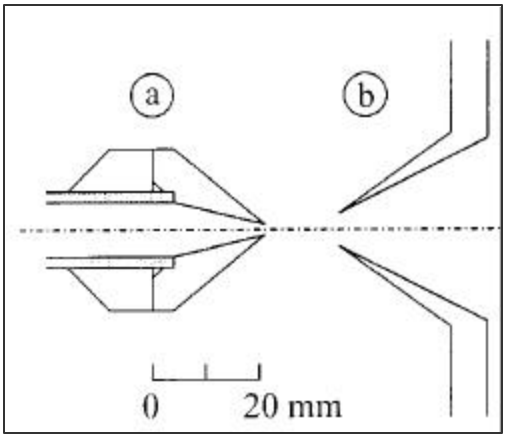

Figure 3.6: *a) nozzle b) skimmer.* **[Nas03]**

Temperature regulation of the nozzle to ~0.1 K is accomplished by comparing the resistance of a resistive heater in the copper block clamped to the nozzle with the

resistance of a calibrated germanium resistor. The output of the comparator is connected to a feedback system that signals the resistive heater to the set temperature.The dissociator and nozzle assembly at the exit side is axially kept in position by means of a mechanical stop. This is an optimum position of the cooled nozzle aperture with respect to the 6 mm diameter skimmer placed 14 mm downstream. Atoms produced in the intense field inside the RF coil escape through the cooled nozzle and are shaped into a beam by a skimmer with an opening diameter of 6 mm (figure 3.6). The skimmer selects the central part of the beam, which is accelerated by the large pressure gradient between the dissociator and the vacuum chamber of the skimmer. The vacuum pressure should be very low to minimize the scattering of atoms before they enter the skimmer. If the pressure is too high *shock waves* are formed that destroys the beam. After the beam is collimated in the skimmer, it proceeds to the sextupole magnets where the electron polarization of the atoms takes place.

A parameter that plays an important role in the analysis of compressible fluids in nozzles is the Mach number. It is defined as:

$$M = v/a, \qquad (3.10)$$

with, a, the local speed of sound and v is the local flow speed of the atoms. The value of a can be calculated by the formula [Dou85]:

$$a = \sqrt{g RT}, \qquad (3.11)$$

where,

g the specific heat ratio,

R the molar gas constant for the atom in $J.mol^{-1}.K^{-1}$,

and T the temperature in Kelvin.

For a converging-diverging nozzle with *isentropic flow* as shown in figure 3.6, the mass flow can be written as:

$$\dot{m} = \rho VA, \tag{3.12}$$

where,

$\dot{m}$ is the mass flow rate,

ρ is the density and A the area through which the atoms move.

Using equation 3.10, taking the logarithm of 3.12 and differentiate it will result in the equation [Dou85]:

$$\frac{dA}{dV} = \frac{A}{V}(M^2 - 1) \tag{3.13}$$

If M < 1 and dA < 0 then dV is positive, it means that the velocity of the atoms increases in a converting-diverting nozzle.

For M = 1,

$$\frac{dA}{dV} = 0 \tag{3.14}$$

This mathematical condition suggests that the area should be a minimum or maximum for M = 1. A maximum for A is not a practical solution but the alternative, a minimum for A, is possible for a converting-diverting nozzle.

In the case of M > 1 and dA > 0, equation 3.13 indicates a movement through the divergent part of the nozzle. Taking these three cases into consideration, gas entering the converting-diverting nozzle with M<1 will be converted to flow from *sub-sonic* to *super-sonic* speeds. The area where M = 1 is called the throat. Under steady state conditions the mass flow rate through the nozzle can be determined in terms of the Mach number and throat area. It can be show that [Dou85]:

$$\dot{m} = \rho AV = \frac{\gamma P_0}{\sqrt{\gamma RT_0}} AM\left(1 + \frac{\gamma - 1}{2} M^2\right)^{\frac{-(\gamma+1)}{2(\gamma-1)}} \tag{3.15}$$

where,

T_0 is the temperature in K and

P_0 is the pressure of the gas at the entrance of the nozzle in mbar.

The maximum mass flow rate for a specific flow area can be obtained by differentiating equation 3.15 with M and setting the resultant equation equal to zero. This condition occurs when M =1. The maximum possible mass flow through the nozzle is therefore obtained when the throat is at the *critical or sonic condition*. The throat is then in a '*choked*' condition and additional gas flow is only possible if the throat is made wider. After passing through the nozzle the atoms move into the zone of silence if M > 1. If the pressure at the exit of the nozzle is low enough this condition will be met. It is in this zone where the skimmer is placed.

3.2.3 Sextupole magnets

These magnets focus the electron-polarized atomic beam for maximum acceptance in the ionizer and deflect the atoms with the unwanted electron spin. An atom in the field of the sextupole magnets acquires two magnetic spin quantum numbers, $m_s = \pm ½$ corresponding to the alignment of the atom either parallel or anti parallel to the magnetic field. The interaction of this non-uniform magnetic field with the magnetic moments of these two states focuses the +½ state and defocuses the -½ state in agreement with the well-known Stern-Gerlach experiment.

Two sextupole magnets, of length 100 mm, are used. The first of the two magnets is 20 mm beyond the exit of the skimmer with diameter tapered from 12.5 mm to 25 mm. The second, with constant diameter of 28.5 mm, is positioned 300 mm further downstream.

3.2.3.1 Selection of states

The magnetic potential for a sextupole magnetic field is given by [Ros92]:

$$j = kr^n \cos nq \tag{3.16}$$

where n, the number of pole pairs is 3, r and q are the cylindrical coordinates.

Thus

$$f = kr^3 \sin 3q \tag{3.17}$$

and the magnetic field in the pole gaps where no current flows:

$$B = -\tilde{N}f \tag{3.18}$$

The various components for the fields are:

$$B_r = -\frac{\partial f}{\partial r} = -3kr^2 \sin 3q \tag{3.19}$$

$$B_q = -\frac{\partial f}{r\partial q} = -3kr^2 \cos 3q \tag{3.20}$$

$$|B| = \sqrt{B_r^{\,2} + B_q^{\,2}} + = 3kr^2 \tag{3.21}$$

The field lines of a typical sextupole magnet are shown in figure 3.7.

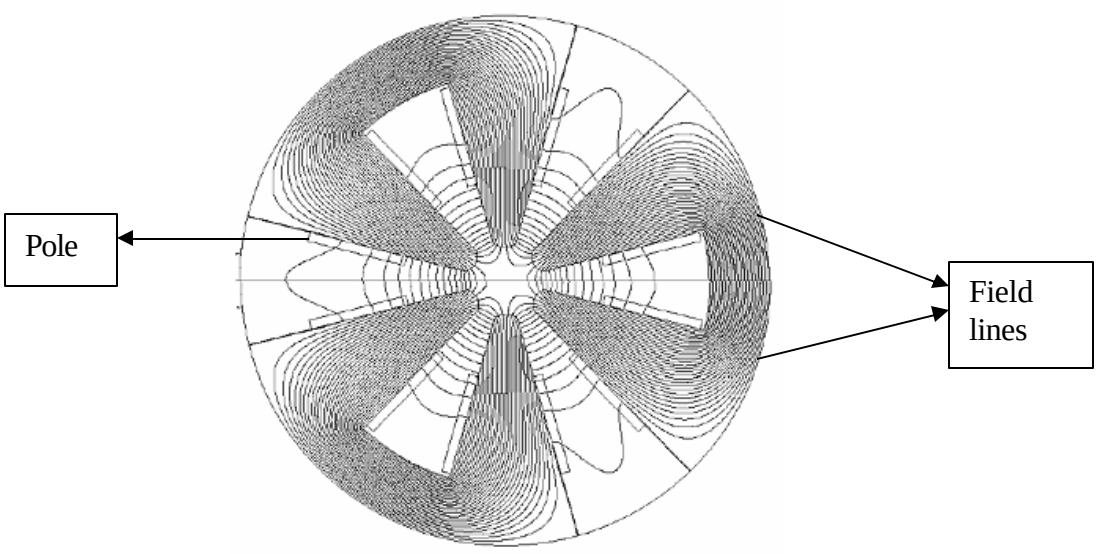

Figure 3.7: *The field lines of a sextupole magnet*.

There is a large concentration of vertical field lines crossing the x-axis near the four poles closest to the x-axis, i.e. horizontal center-line of the magnets. The field has a high value at these points but at the center of the magnet there are no field lines. This illustrates the parabolic nature of the vertical field between the poles in correspondence with the equation 3.21 and is depicted in figure 3.8.

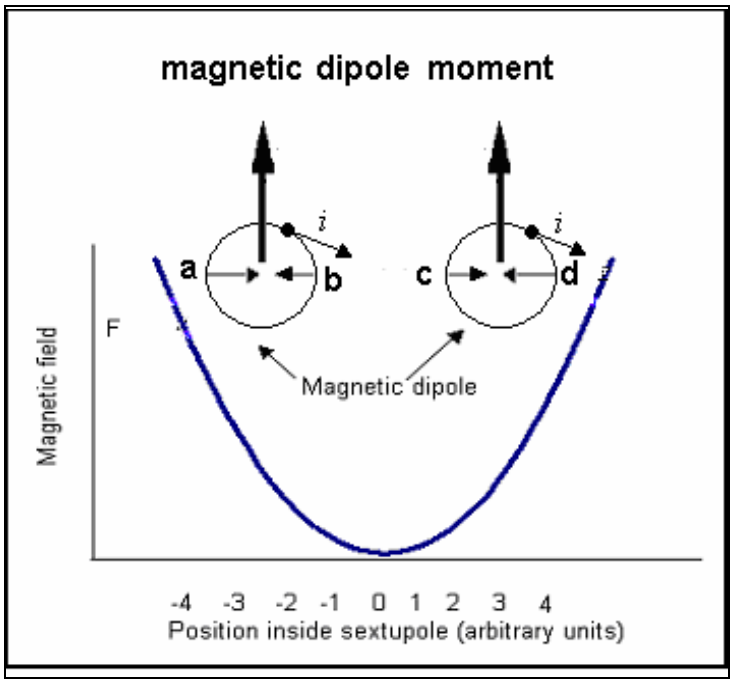

Figure 3.8: *A schematic diagram illustrating the focusing effect of the sextupole magnet on a magnetic dipole. The magnetic field units are arbitrary and the position inside the sextupole is along the horizontal center line of the magnet or along the x-axis.*

The circles in figure 3.7 illustrate magnetic dipoles in a magnetic field representing the electron magnetic dipole of an atom. The current in each dipole is shown as well as the direction of the magnetic moment indicated by the bold arrows. The field at ‘a’ in the sketch is higher than the field at ‘b’ therefore the force at ‘b’ directed to the left is smaller than the force at ‘a’ directed to the right. The net force is therefore towards the center. The same argument applies for the dipole at the right. If the currents through the dipoles were reversed the net force would be directed outward. The first case illustrates the focusing effect and the second a defocusing effect of an electron spin dipole. It is obvious

that the force will deflect the + state to the left and the – state to the left. The energy of the dipole is:

$$W = -\vec{m}.\vec{B} \qquad (3.22)$$

and the force:

$$F = -\vec{m}.\nabla\vec{B} \qquad (3.23)$$

$$F = -\vec{m}.\frac{\partial 3kr^2}{\partial r} \qquad (3.24)$$

$$F = m\ddot{r} = -\vec{m}.6kr \qquad (3.25)$$

The separation of the two states is caused by the interaction of the magnetic moments of the states and the inhomogeneous field of the sextupole. The trajectory of atoms through a sextupole for the various magnetic quantum states is shown in figure 3.9.

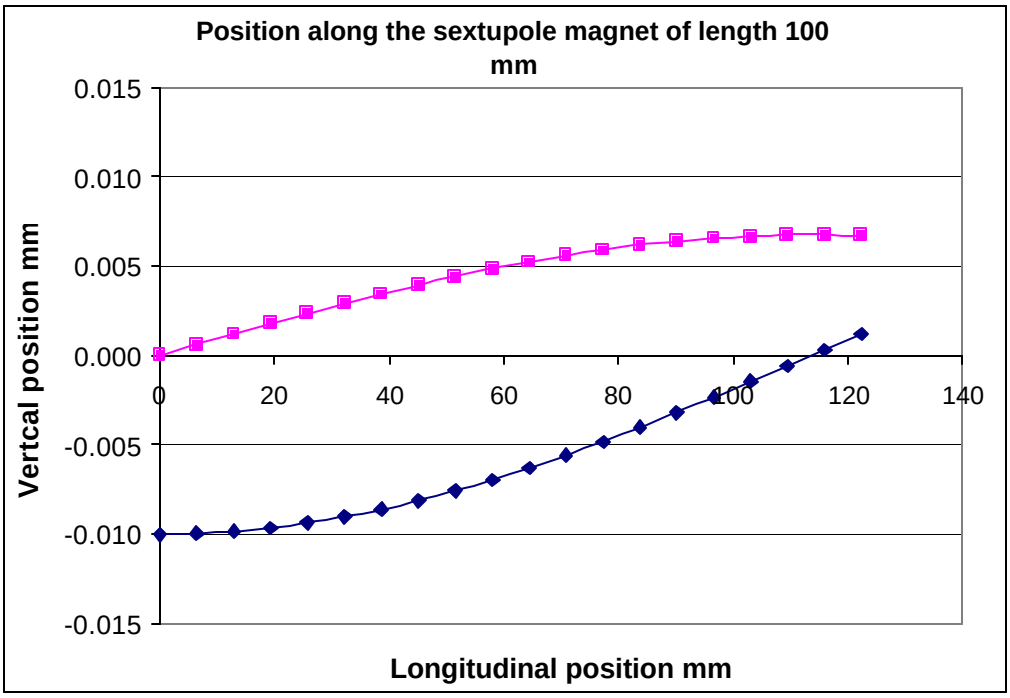

Figure 3.9: *The motion of two atoms with an electron spin of +1/2 along the sextupole magnet for various positions at the entrance of the magnet.*

3.2.4 Nuclear Polarization

The beam passes through two RF transition units called the weak field (WF) and strong field (SF) units (see figures 3.10, 3.11 and 3.12). RF transitions are selected to populate specific hyperfine levels inside the atom. The high frequency field of the SF is generated by a strip-line resonator and for the WF the field is generated in a coil. The frequency for a SF is 1450 MHz and the magnetic field is ±150 Gauss while the frequency and the field for the WF is 10 MHz and 6 Gauss respectively. For the transitions to take place the correct RF frequencies as well the correct constant magnetic field inside the transition units must be set. The correct tuning of the WF unit will result in a transition between quantum state 1 and state 3 and will cause the depopulation of state 1 and population of state 3. The nuclear quantum number m_I for both states 2 and 3 are $-½$. Therefore the polarization is defined as $P_z = -1$. Tuning the SF unit will result in a transition between quantum state 2 and state 4 and will cause the depopulation of state 2 and population of state 4. The m_I quantum number for both states 1 and 4 are ½. It follows that the beam is now in a $P_z = +1$ polarization state.

Classically it means that when the two transition units are alternatively switched on and off the nuclear magnetic moment flips through 180^0 [WWW1].

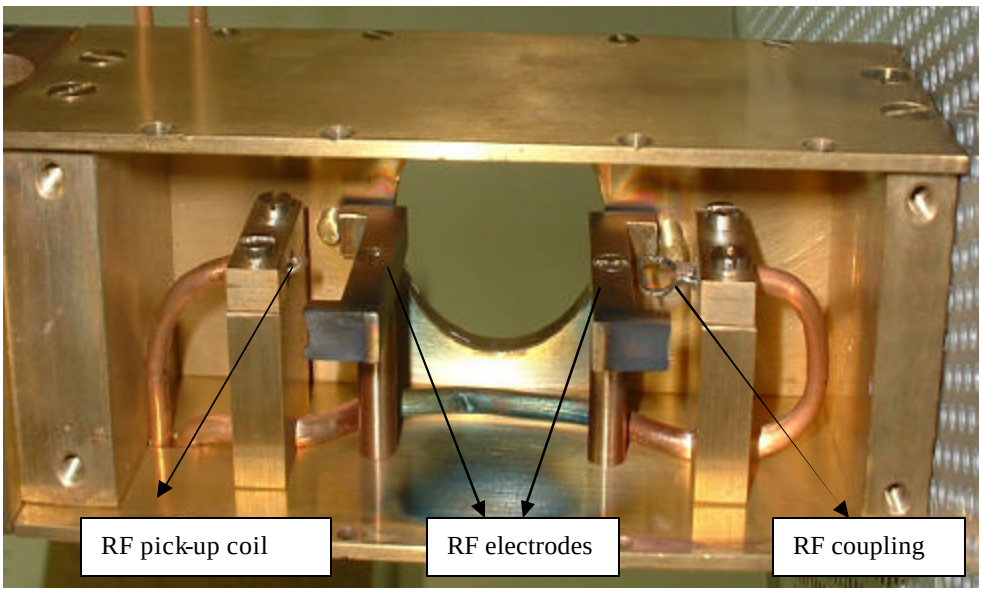

Figure 3.10: *The strong field RF unit.*

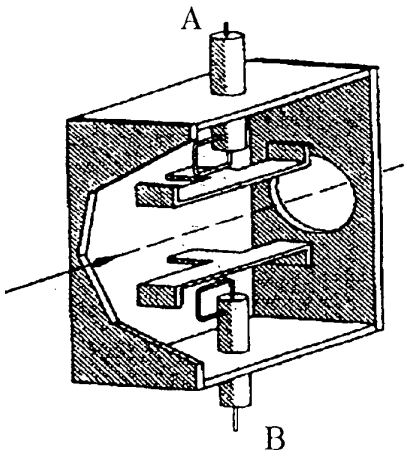

Figure 3.11: *Cavity for the strong field unit* (1.4 GHz)

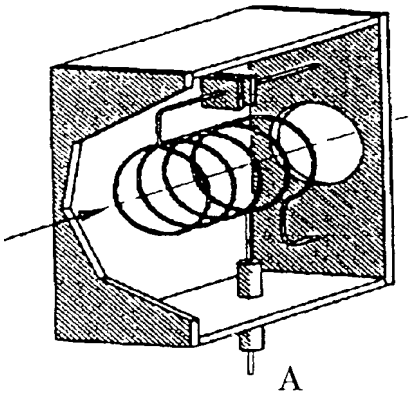

Figure 3.12: *Coils for the weak field unit (10 MHz)*

The beam enters the strong field unit at the aperture and passes the two RF electrodes (shown in figure 3.10). The electrodes are 6x6 mm^2 copper bars at the end of a 6 mm copper tube connected to the ground. These electrodes form for a $\lambda/4$ resonator. The RF from the power supply is inductively coupled as can be seen on the copper pillar on the right of the photo. The reflected power is measured by means of the inductive loop at the column on the left side of the photo. The semi-rigid cables from the RF generators are

visible in the photo (figure 3.10). The setting of the RF at the given values the polarization can be established by using the Jachard method (see Chapter 5).

3.2.5 The Ionizer

The ionizer used at iThemba LABS is a strong-field ionizer. This type of ionizer requires an RF transition apparatus to induce radio frequency transitions between hyperfine states of the atomic beam before ionization. If this condition is not met zero polarization results. The advantage of this ionizer is that it offers higher polarization and electrons are confined by the magnetic field creating a long electron path length through the atomic beam [Gla68].

A tantalum filament inside the ionizer emits electrons that are accelerated and ionizes the beam in the ionization chamber. Ionization of neutral atoms by collisions is called electron impact ionization. The ionization chamber is a long tantalum tube housing various high voltage electrodes having various functions. Figure 3.13 shows a picture of the ionizer. Electrodes extract and repel electrons emitted by the filament and also accelerate and focus protons (see the schematic diagram, figure 4.16). The length and shape of the filament are some of the important factors that influence the beam intensity (discussed in Chapter 4). The filament is heated by sending a direct current with a maximum value of 20 A for thermionic emission of electrons.

The electrons escaping from the filament are accelerated by an applied electric field to an energy that is sufficient to cause ionization when they collide with the atoms. The electron energy must exceed the energy needed to remove the outermost bound electron from the neutral atom, called the ionization potential (ϕ), or $E_e > e\phi$ [Bro89]. For hydrogen the energy is 13.6 eV [Yar60]. The ionizer ionizes the beam thus producing a proton beam. Figure 3.13 shows a picture of the ionizer.

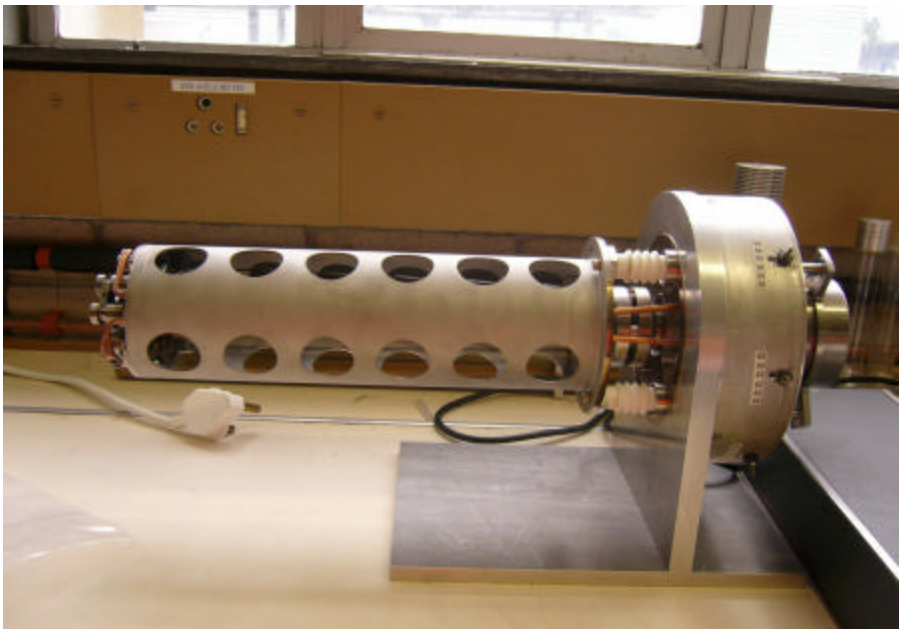

Figure 3.13: *Photo of the ionizer. The magnetic field of the ionizer, created by a solenoid around the cylinder shown in the figure, confines the electrons to the ionization column. The metal shield prevents scattered atoms from entering the ionizer.*

The electron current density for this filament can be calculated using the Richarson-Dunshman equation [Bro95]:

$$j_e = A\,T^2\,e^{-\frac{eW}{kT}} \qquad (3.26)$$

with,

$$A = \frac{4p\,emk^2}{h^3}$$
$$= 120\,A/cm^2$$

where,

A is the Richardson constant,

W is the work function of tantalum (see appendix C),

e is the electron charge,

k is the Boltzmann constant, and

T is the temperature of the filament in Kelvin.

Electrodes in the ionizer direct the electrons from the filament to the ionization chamber where they are confined by electrodes on either side of the plasma chamber and by the magnetic field. These electrodes are at a negative or positive potential depending on their function. The beam enters the ionizer from the left hand side through the hollow filament (figure 4.16). The beam then passes through the ionization chamber and exits it on the right hand side.

3.2.6 The pressure chamber for measuring the dissociation of hydrogen gas

This device consist of a stainless steel tube with an 1.2 cm inside diameter and 10 cm long followed by a 200 cm^3 stainless steel chamber in which the pressure is monitored by a Bayard-Alpert gauge. This entire system is mounted with its entrance tube aligned with the beam axis at a position beyond the first nuclear RF transition unit.

The number of particles per second collected in the pressure tube causes a rise in the pressure that is measured by the vacuum gauge. Calibration of the number of particles required to cause a given pressure rise in the compression chamber was accomplished by measuring the pressure rise for a known, small flow of H-gas into the chamber. A consistent calibration was obtained when care was taken to eliminate leaks and unwanted gases. This device is used to determine the atomic beam flux by measuring the pressure difference when the tube captures the beam and when the tube is moved out of the beam. This pressure difference is also used to determine the ionization efficiency of the beam as well as the dissociation degree.

CHAPTER 4

OPTIMIZATION OF THE ION SOURCE

4.1 Introduction

The optimal functioning of the ion source and the intensity of the beam that is produced depend on a number of factors that were stated in chapter 3. These factors were studied and methods of optimizing the beam current were established. Experiments were done to investigate different methods that could be used to optimize the beam current. All these factors are discussed and the results will be shown in this chapter.

4.2 Low-temperature effect and nitrogen gas

4.2.1 Low-temperature effect

After the molecules have been dissociated into atoms, they move through the nozzle, which is fitted at the end of the Pyrex tube. The nozzle is cooled down by a two-stage helium refrigerator to a temperature of approximately 30 K. The beam is therefore also cooled down by the nozzle to approximately the same temperature. The temperature of the cold head is controlled by the temperature controller unit and the current is measured by a faraday cup after the 100^0 magnet that is situated after the beamline solenoid. As the atoms are cooled down from room temperature to lower temperatures the beam intensity increases. When the temperature is low enough (less than 30 K but greater than 27 K), the velocity of the beam becomes smaller and the recombination of the atoms decreases, therefore increasing the beam intensity. Figures 4.1 and 4.2 illustrates how the lowering of the temperature affects the measured current and the dissociation degree.

4.2.1.1 Results and discussion

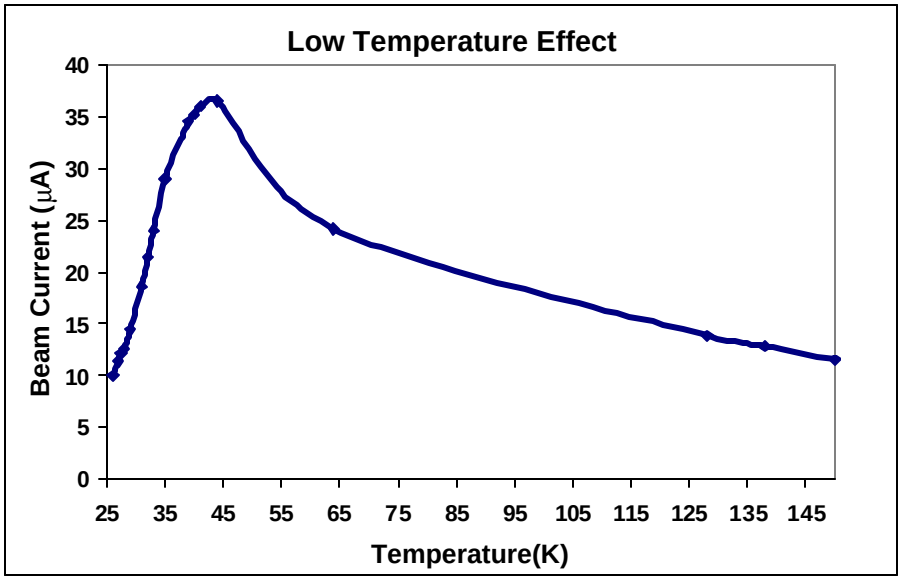

Figure 4.1*: Beam Intensity as a function of temperature. The resistance of the filament used in this experiment is 22 mW and the cross-section of the Cu nozzle 7.5 mm.*

At low temperatures the beam current increases because the velocity of particles in the beam is decreased, which reduces the chances that the dissociated particles can collide and recombine. This increases the number of dissociated particles (dissociation degree) that can be ionized to form a proton beam, but it was observed that at very low temperatures, below 40 K, the beam intensity decreases (figure 4.1). This occurs because the particles are moving at a very low velocity causing the atoms to spend more time in the nozzle. The longer the particles remain in the nozzle, the greater the probability of recombination and the lower the beam current. This is caused by particles colliding with the walls of the nozzle and recombining to form hydrogen molecules therefore decreasing the number of atoms that can be ionized. This causes the beam current to decrease.

Figure 4.1 shows that when the temperature reaches ~31 K the beam current decreases rapidly, by almost 50%. As the temperatures decreases further, beam current continues to decrease. At approximately 25 K the beam current is less that its initial value (i.e. less than 10 μA). From these results it can be deduced that decreasing the temperature has a

positive effect on the beam current until a temperatures of ~40 K has been reached. Below this temperature the beam intensity decreases.

Figure 4.2 shows the effect of temperature on the dissociation degree.

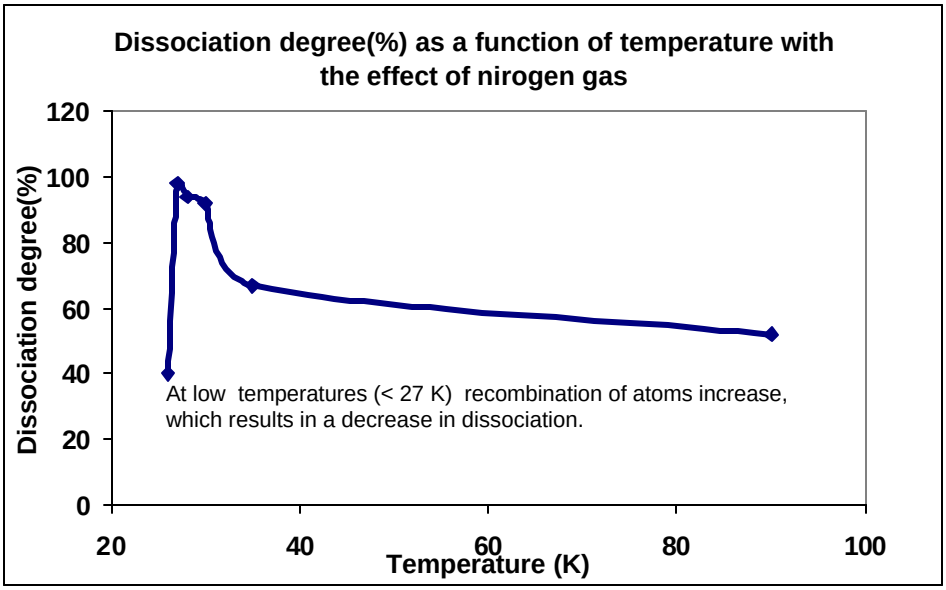

Figure 4.2: *The graph shows the influence of temperature on the dissociation of particles into atoms. These results were obtained by measuring the atomic beam flux using the compression tube and then using equation 3.2 to calculate* a.

We notice that the dissociation degree only decreases at much lower temperatures (< 30 K). This is due to the use of nitrogen gas at low temperatures to prevent recombination of atoms. This is discussed in the following section (4.2.2).

4.2.2 The effect of nitrogen gas

From previous experiments, it is well known that the intensity of the beam can be enhanced if monatomic nitrogen gas is sprayed into the entrance of the nozzle at temperatures between 39 K and 35 K. It is sprayed before or when the low temperature starts having a negative effect on the beam current (beam current decreases). This is done

to prevent recombination of atoms. Nitrogen gas deposits on the walls of the nozzle to prevent the atoms from colliding with the walls of the nozzle. When atoms collide with the walls they readily recombine. Figure 4.3 illustrates the effect of nitrogen gas on the decreasing beam intensity at low temperatures. The results of this measurement are collected in a graph of beam current as a function of temperature combined with the effect of nitrogen.

4.2.2.1 Results

Nitrogen gas might increase the beam intensity by ~100 % although the amount of nitrogen sprayed has also an optimum value beyond which the beam intensity drops. From the time when nitrogen gas is sprayed in the nozzle, the beam current increases with decreasing temperature, i.e. beam current is inversely proportional to temperature.

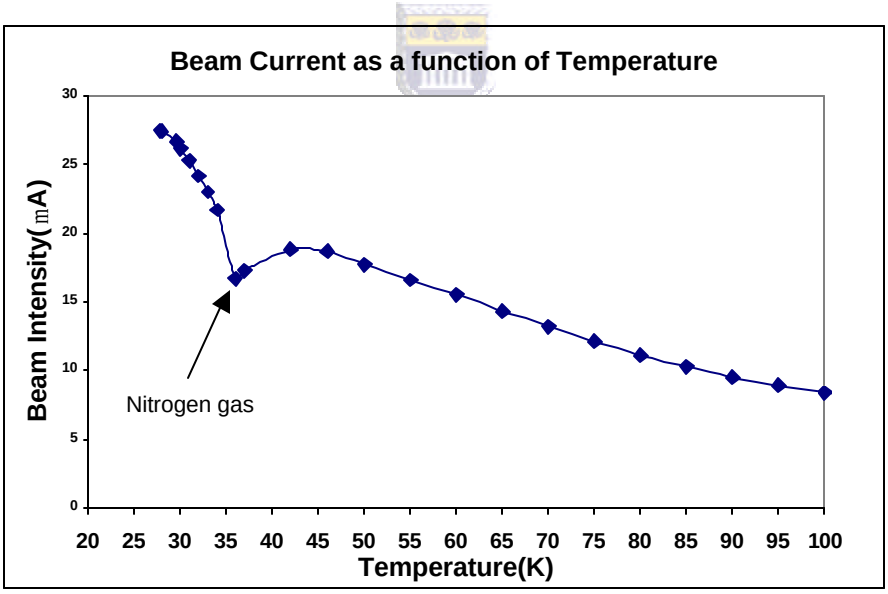

Figure 4.3*: Graph depicts the effect of nitrogen on the beam intensity.*

Figure 4.3 shows that beam intensity increases with a decrease in temperature until approximately 40 K, after this the beam current decreases. As soon as nitrogen gas is sprayed on the entrance of the nozzle, the beam intensity increases. Figure 4.4 depicts the

results of measurements, which were done to investigate the effect of nitrogen gas at different temperatures.

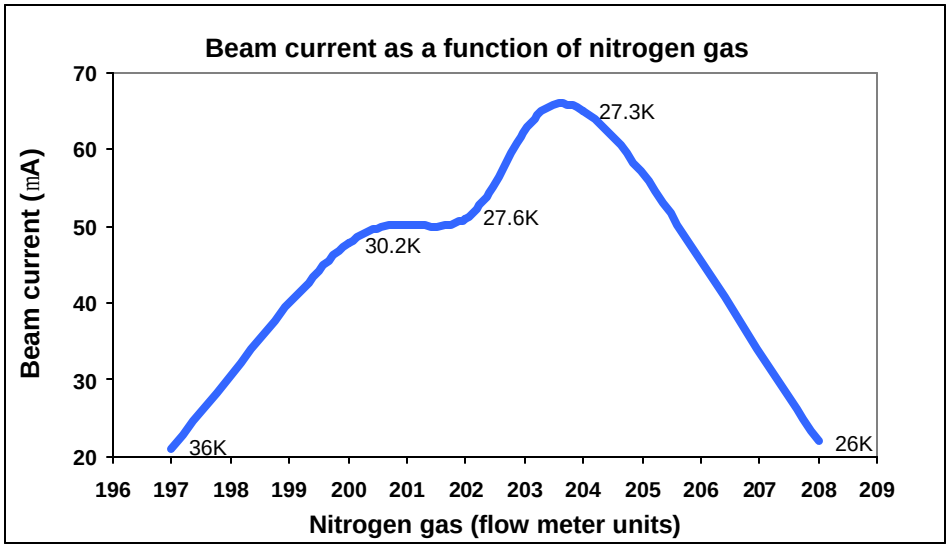

Figure 4.4: *A 22 mW filament was used for this experiment and a copper nozzle with a cross-section of 11.5 mm. The temperature of the beam decreased automatically with the nozzle temperature while the amount of nitrogen had to be varied to obtain optimum beam current at each temperature reading.*

Results indicate that:

- At lower temperatures (<36 K) more nitrogen is required than at higher temperatures i.e. the amount of nitrogen gas required to increase beam intensity increases with a decrease in temperature. When the nitrogen valve is opened (usually between 39 and 36 K), the valve is turned to approximately 200 divisions on the flow meter scale, but as the temperature decreases the valve is opened further to increase the flow of nitrogen gas into the nozzle in order to increase the beam current. As the temperature decreases further, the amount of nitrogen gas should be increased. Beam current is almost 70 μA at 27.3 K using 204 valve divisions as compared to the 47.73 μA at 30.2 K using 200 divisions (figure 4.4). Optimum beam current is obtained at 204 divisions, after that the beam current starts to decrease with the temperature. As the temperature decreases below 27 K

recombination of atoms increases even when the amount of nitrogen gas is increased. At 26 K the velocity of the particle is too low and nitrogen particles become more and the atoms collide with the nitrogen particles resulting in a decreased in beam current. This leads to the conclusion that the effect of nitrogen on the beam current is largely influenced by temperature, the lower the temperature, the bigger the amount of nitrogen gas required.

- At lower temperatures (less than 26 K) the amount of nitrogen gas used caused the beam current to decrease. This is caused by more collisions of the beam particles with nitrogen particles. A large amount of nitrogen gas also restricts the entrance of the nozzle decreasing the pressure gradient between the entrance and the exit of the nozzle that is required to expand the beam when it exits the nozzle. From this we can deduce that nitrogen gas has an optimum value, above which value the beam current will decrease.

The effect of nitrogen gas was also investigated using two different filaments to determine if the effect varies from one filament to another (figure 4.5). The results show that the effect of nitrogen is the same for both filaments. Filament 2 shows a higher peak in the figure than filament 1 due to its higher resistance and larger area, but the shape of the graph is the same. The reason for the different peak values will be discussed in the section on filaments (Chapter 4.6).

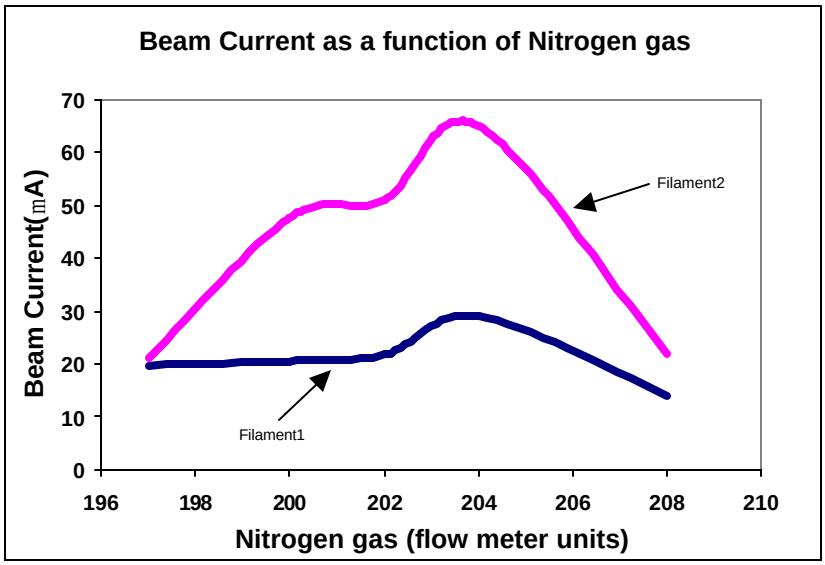

Figure 4.5: *Beam current as a function of gas flow for two different filaments. Filament 1 has a resistance of 17 mW and filament 2 has a resistance of 22 mW.*

4.2.3 Conclusions

Beam current is inversely proportional to the temperature up to an optimal temperature. During this measurement the optimum temperature was 39 K, from where the beam intensity decreases with temperature.

The lower the temperature the bigger the amount of nitrogen needed to prevent recombination up until the optimum temperature (figure 4.4).

There is an optimum value for nitrogen, beyond which the beam current decreases.

Nitrogen gas flow and the temperature effect are a combination that is important in increasing the beam intensity. The temperature should be used as an indication of the amount of nitrogen required to increase beam intensity. When the correct amount of nitrogen gas is used at a suitable temperature, optimum beam intensity is achievable. The temperature should be kept between 30 K and 27 K while the nitrogen gas flow should be used according to the temperature (between 200 and 208 divisions on the flow meter) to achieve optimum beam current.

When there is excess nitrogen in the nozzle, the nozzle should be warmed up to temperatures above the boiling point of nitrogen (> 73K) to get rid of all the nitrogen in the nozzle. After that the procedure to optimize the beam current should be started again.

4.3 Calibration of the pressure tube

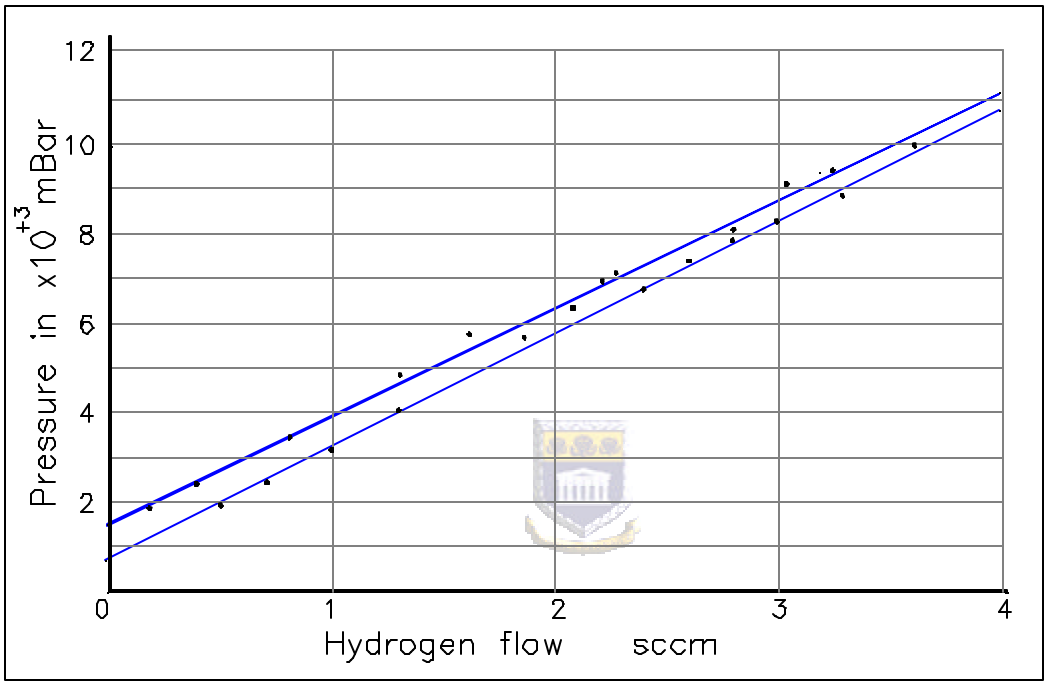

Figure 4.6: *The relation between the change in pressure and the flow of hydrogen atoms into the pressure tube. The calibration leads to 1.86 x10 ^{20} atoms/s/mbar.*

The pressure caused by this stream of particles can be measured in the pressure tube. The increase of pressure in the pressure tube is an indication of the influx of particle flux from the dissociator. To calibrate the pressure tube, the rise in pressure is measured by means of an Alpen-Bayern hot gauge and the flux of particles by measuring the flux in $sccm^{-1}$ (cm^3/min) at the flow meter. From the graph (Figure 4.6) the ratio between pressure in mbar and flow in $sccm^{-1}$ is 2.37×10^{-3} mbar per $sccm^{-1}$. This relates to 1.86×10^{20} atoms/s/mbar by calculating the flow in atoms/sec as follows:

$$PV = nRT \qquad 4.12$$

$$\therefore PS = \dot{n}kT$$

$$\dot{n} = \frac{PS}{kT}$$

therefore:

$$\dot{n} = 4.42 \times 10^{17} atoms/\text{sec}$$

where: n is the number of moles,

k is the Boltzmann constant in $J\ K^{-1}$,

T is room temperature in K, P is standard pressure,

V is the volume of gas in $sccm^{-1}$,

S is the flow of gas per second.

4.4 Effect of gas flow and dissociator power

The amount of H_2 gas flowing into the dissociator influences the final beam intensity. The bigger the amount of hydrogen gas, the bigger the number of particles that are dissociated. The dissociation of particles also depends on the amount of power from the generator. When the gas flow is high, the power used for dissociation should also be high to ensure that a large percentage of the particles is dissociated. For a gas flow of about 19 to 21 sccm (cm^3/min), power of 100 Watts is sufficient for optimum dissociation. For a high gas flow, more power is required to produce optimum results.

Figure 4.7 shows the relationship between beam current and the amount of power that is used. The graph shows that the relationship between beam current and the power is directly proportional, an increase in power leads to an increase beam current. The beam

current reaches a plateau at approximately 120 W beyond which an increase in power will make little difference on the beam current.

4.4.1 Results

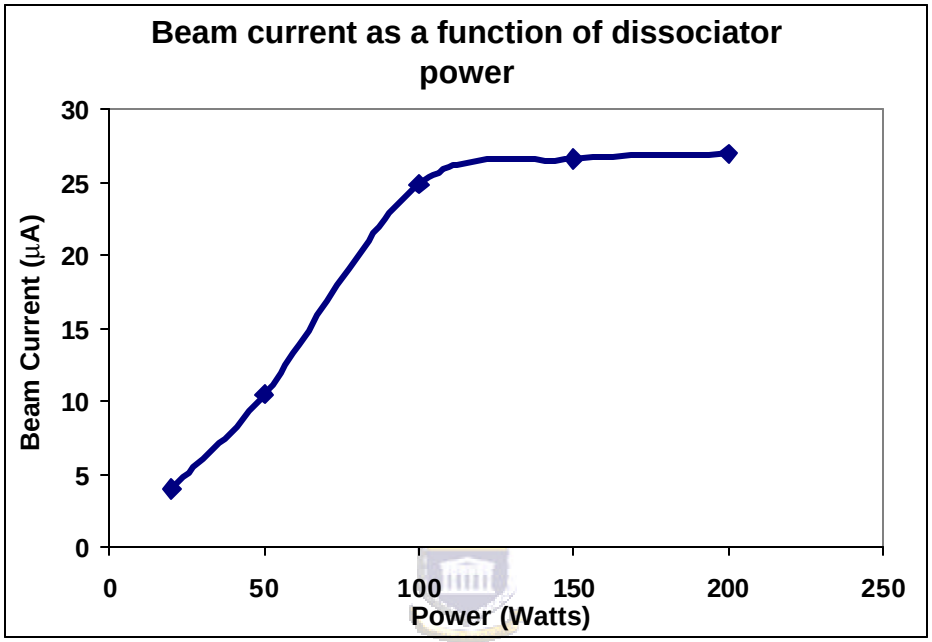

Figure 4.7: *The dependence of beam current on the power from the generator. Measurements were done at a constant hydrogen gas flow of 20.2 sccm and a filament current of 16.57 A, with the voltage at 5.9 V. The temperature was kept constant at 39 K. The measurements were taken without the influence of nitrogen gas.*

4.4.2 Discussion

Results indicate that:

1. A high gas flow requires a high rf power to heat up the molecules thereby, increasing the dissociation of the molecules into atoms.
2. A high dissociation degree increases the beam intensity because a large number of particles are dissociated into atoms, which are then ionized in the ionizer.

3. Dissociation is also influenced by the temperature of the particles in the beam (see Figure 4.2). At low temperatures the dissociation degree decreases due to an increase in recombination of atoms.

The flow of hydrogen into the dissociator also affects the pressure inside the dissociator. Caution has to be taken when increasing the gas flow because it increases the pressure inside the dissociator and its vacuum chamber. When the hydrogen gas starts flowing inside the Pyrex tube, the pressure increases from $4x10^{-7}$ mbar to about 10^{-5} mbar in the dissociation chamber, and to 3×10^{-6} mbar in the sextupole chamber. The pressure inside the ionizer should not exceed 4×10^{-7} mbar. The presence of hydrogen molecules in the ionizer vacuum system can be a source of un-polarized background.

To obtain optimum results, the pressure (both in the dissociator and in the ionizer) has to be kept as low as possible. A useful method of keeping the pressure low is to increase the pumping speed. It is also an advantage to use small amounts of hydrogen as possible for a required beam current. For most beams a gas flow of 22–24 $sccm^{-1}$ is used. Larger amounts of hydrogen require more power to dissociate particles.

4.5 Rf of the dissociator

4.5.1 The Impedance Matching box

The energy needed for the dissociation is supplied from a 13.6 MHz generator with a maximum power of 500 W. The generator is connected to the dissociator coil via a 50-ohm (TR 115U) cable. A LRC circuit, called a impedance matching box, is inserted between the source and the dissociator coil to couple energy from the generator to the plasma. Figure 4.8 depicts a diagram of this connection.

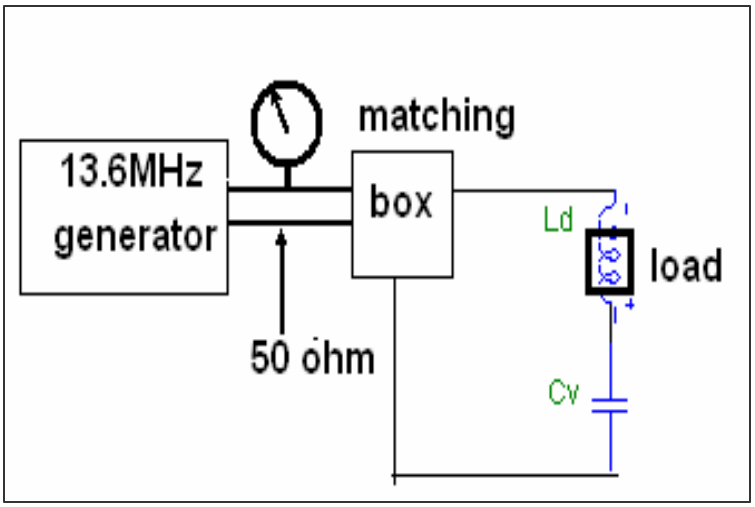

Figure 4.8*: The connection between the power supply and the load***.**

The purpose of the RLC circuit/matching box is to make the load non-reflecting at 13.6 MHz. In order to do this the input impedance of the ion source must be transformed to 50 Ω to match the output impedance (50 ohms) of the generator and the cable. Figure 4.9 shows the electrical elements inside the box.

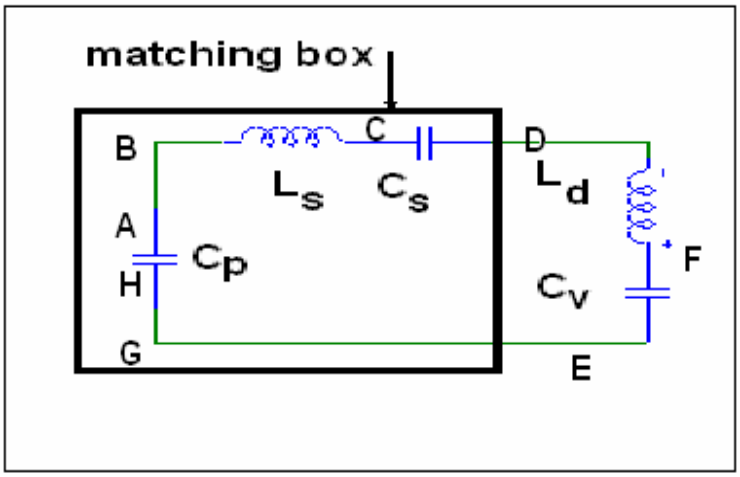

Figure 4.9: *Elements of the matching box as well as the vacuum capacitor and dissociator inductor.*

The effective transfer of RF power to the dissociator is made possible by tuning the three variable capacitors shown in the figure and monitoring the reflected power by a reflectometer. It was soon realized that the variable parallel capacitance, C_P in Figure 4.9, had reached the end of its maximum range and could therefore not be tuned to bigger values. It was impossible to tune the beam for minimum reflective power during optimizing the source. At an output RF power of 120W the reflected power was ~30%. This resulted in a beam with low intensity because of the ineffective process of dissociation.

An investigation with a Hewlett-Packard Vector Impedance Meter (VIPM) showed that the load seen by the generator was 84 ohms at 13.6 MHz instead of 50 ohms. A solution was to add a parallel capacitance C_{PA} to the existing parallel capacitance C_P.

In order to determine the value of this new capacitor (C_{PA}) the components of the matching box as well as the inductance coil and vacuum capacitor outside the dissociator were uncoupled where possible in order to measure their values. The stray values associated with all these components as well as the inductances in the leads of the VIPM were directly or indirectly measured or calculated. With this knowledge it was possible to use the program MICRO-CAP, or any other network-analyzing program to determine a value for C_{PA} that will match the load of the source with the characteristic impedance of 50 Ω. C_{PA} should be a variable capacitor so that 50 Ω will be reached with the capacitance of the capacitor C_P in the midrange of its scale.

It was impossible to isolate all the components in order to measure them. Isolation of capacitors and inductors could only in some cases be done in combination. For instance, to calculate C_p and L_s the point C was earthed. C_p and L_s was now considered as parallel. By earthing B and D would make L_s and C_s parallel. L_d and C_v could be isolated by unscrewing them. It was also possible to measure or calculate the stray capacitance, stray inductance and resistances. For instance, the inductance between G and H and the capacitor C_p could be considered to be in series by earthing point A.

The following procedures were followed to determine the values of isolated components or combination of isolated components.

1. If the components (actual or stray) were in series, the inductance (L) of the inductor could be calculated by measuring the series impedance of the connection using the VIPM at high frequencies.

   It is clear from the equations:

$$X_l = Lw \text{ and } X_C = \frac{1}{Cw}, \qquad (4.1)$$

   that only X_l will contribute to the total series impedance and that X_c will be insignificant small. The value of L can be calculated from 4.1. A typical graph of reactance versus frequency is shown in figure 4.10. From this graph the inductance can be calculated.

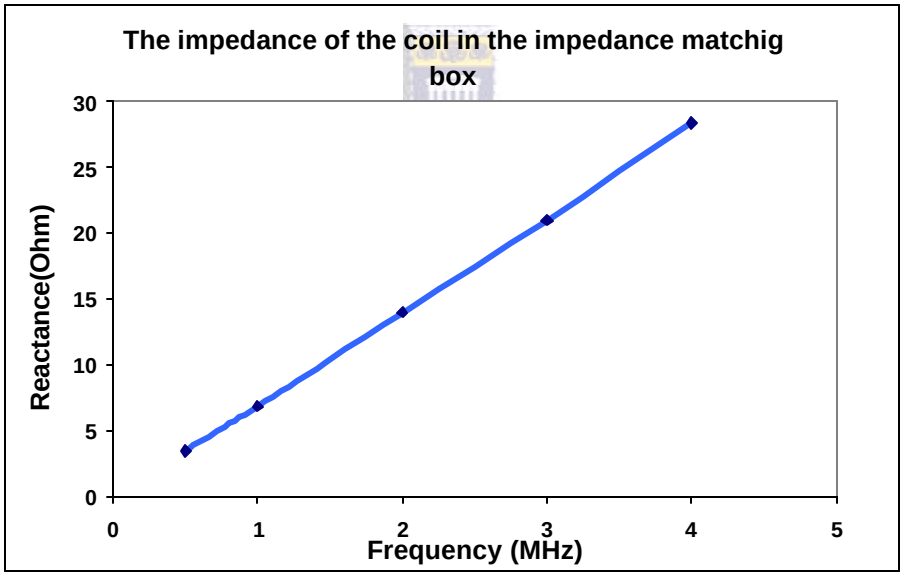

Figure 4.10: *Frequency dependent impedance of an inductor*.

In the same way the capacitance could be obtained by measuring the impedance of the connected elements using the VIPM at low frequencies. The impedance of the inductance can be neglected because it is considerably smaller than the impedance of the capacitance at low frequencies. A typical graph of reactance

versus frequency is shown if figure 4.11. The capacitance could therefore be calculated using a measurement at low frequencies.

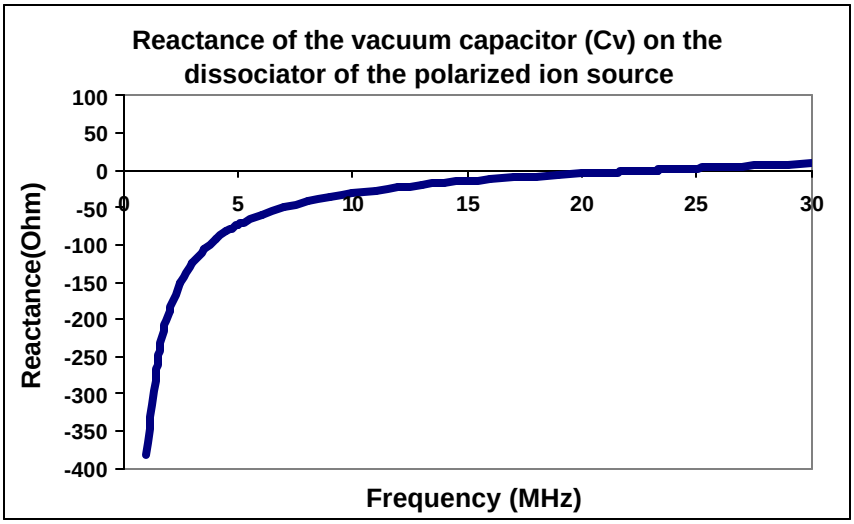

Figure 4.11*: Reactance of a capacitor as a function of frequency.*

In order to confirm the values obtained from the above-mentioned proceedings an additional measurement was done by combining components to obtain series resonance. A typical graph of reactance versus frequency for a series resonant circuit is shown in figure 4.12.

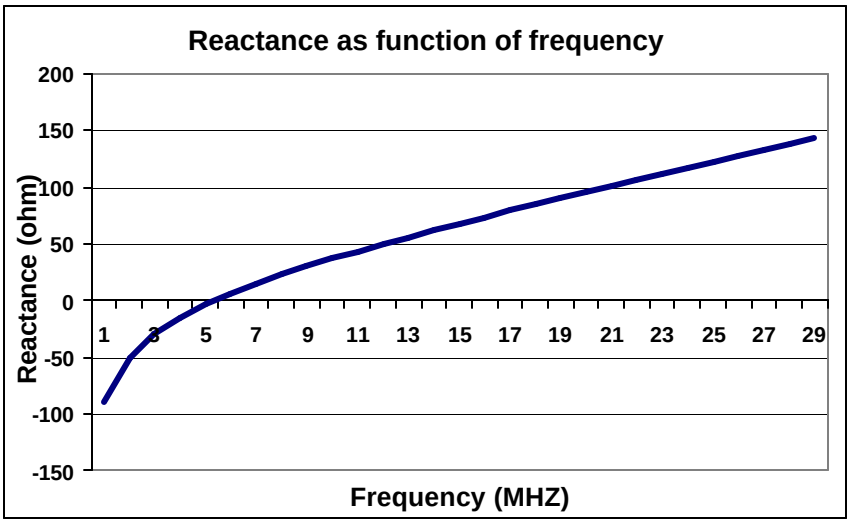

Figure 4.12*: A graph of reactance versus frequency for a series resonant circuit.*

At series resonance the impedance is zero. Therefore

$$X_l = X_c \qquad (4.2)$$

The values of L and C can be confirmed using the equation 4.1,

2. If the components were parallel coupled (e.g. the dissociator coil and vacuum capacitor) the frequency of the VIPM was tuned to obtain resonance. By obtaining resonance at another frequency and another known value of the capacitance, two simultaneous equations could be found that will give a solution for L and C. The value of L or C must first be calculated at these frequencies using the procedure 1 above.

At resonance:

$$Lw = \frac{1}{Cw} \qquad (4.3)$$

3. The resistance was measured at parallel resonance at a convenient frequency on the VIPM and then scaled using the inverse square root of the frequency f. The reason for this is that the penetration depths d inside copper conductors is responsible for resistance and formula for it is given by:

$$d = \frac{.0661}{\sqrt{f}} \text{ m} \qquad (4.4)$$

4. The leads of the VIPM as well as the cable or wire interconnections have capacitance and inductance. The impedance of these elements were measured and deducted from the impedance measurements as described above.

5. Stray parallel capacitance of the inductors was calculated by doing an impedance measurement when the frequency is at resonance. The stray capacitance can be calculated because the inductance is known from previous measurements (see 1).

4.5.2 Discussion

After obtaining the values for all the elements a complete circuit diagram of all the elements was used as an input in the MICRO-CAP program. Figure 4.13 shows this diagram. Varying the frequency, tuning the values of the variable capacitance and analyze the real and imaginary values of the voltage after the power supply it was possible to have resonance at 13.6 MHz and a load of 50 Ω. Figures 4.14 and 4.15 depict the results of graphs. From this the value of the second parallel capacitor should be 70 pF. A variable capacitor with maximum capacitance of 200 pF was procured and tested to 1500 V. It was installed into the matching box and tested. The reflected power was zero at 120 W. The benefit of this enhancement is that the input power to the dissociator can now be much higher with the result of increasing the dissociating factor. Beam current will be higher. Experiments were done and the beam intensity showed an increase of about 10%.

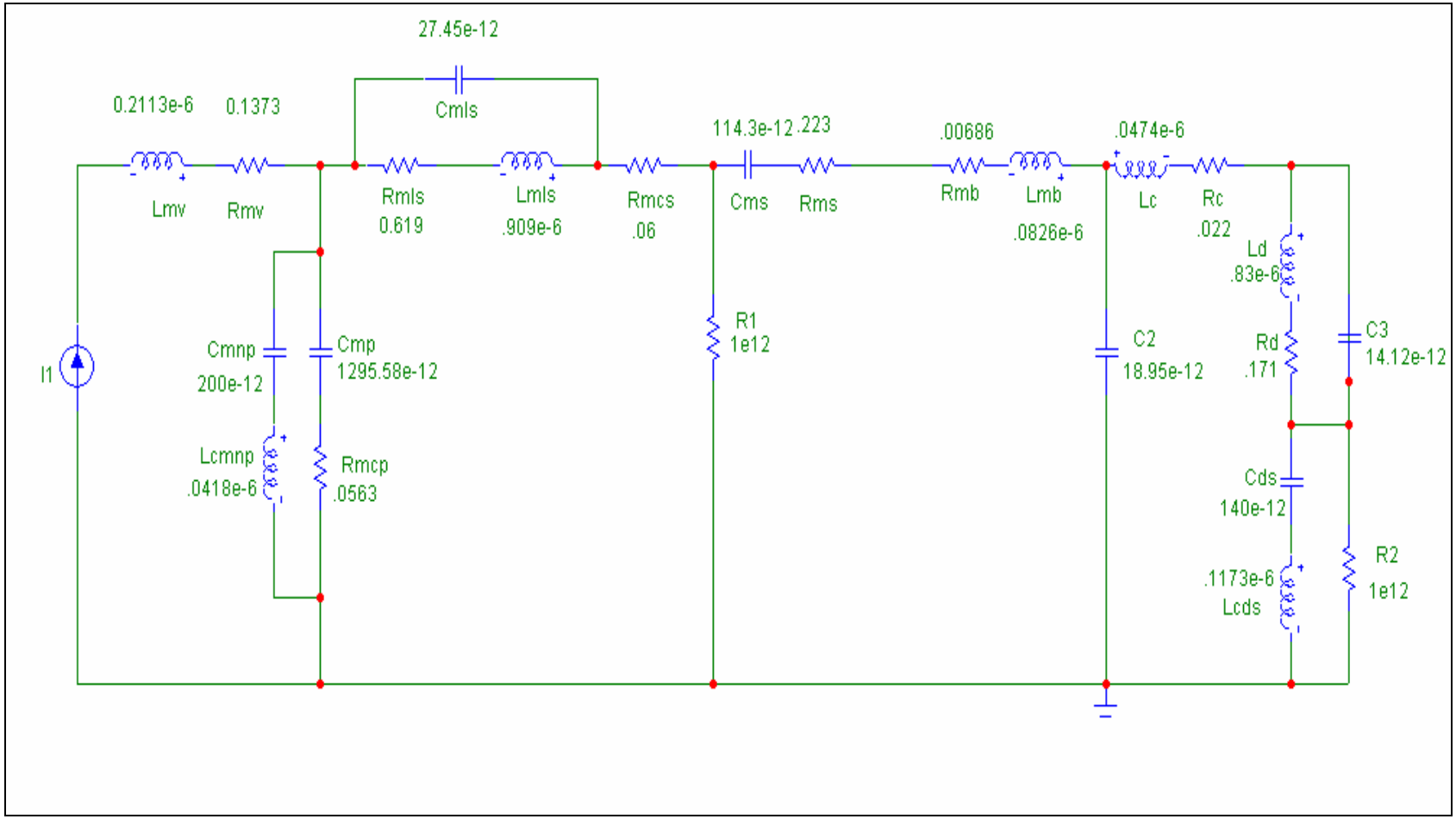

Figure 4.13: *Circuit diagram of the impedance matching box, the dissociator coil and the vacuum capacitor. The circuit shows the values of all the components and stray components.*

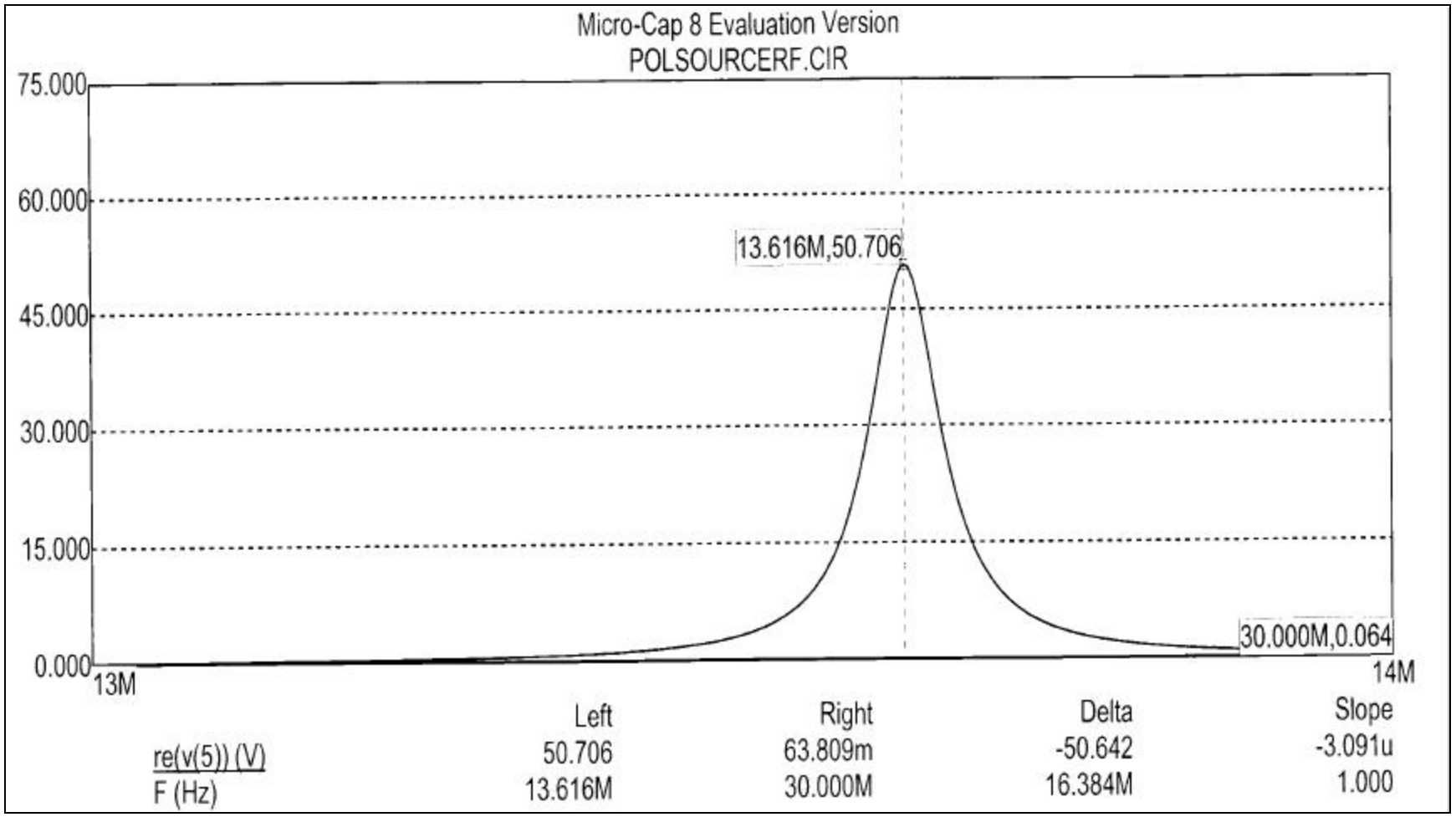

Figure 4.14: *Resistance of the LRC circuit as a function of frequency at and near the resonance frequency.*

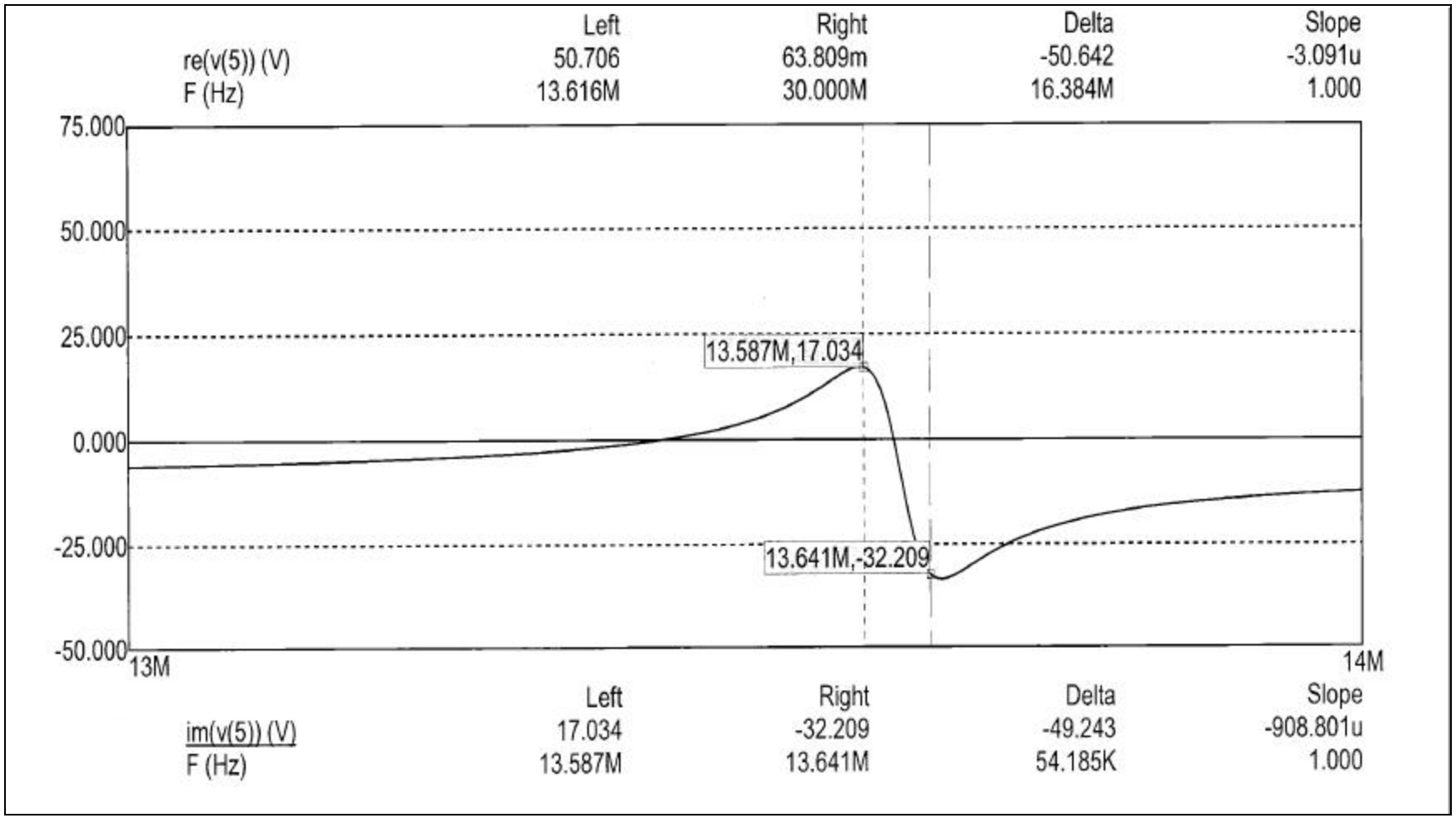

Figure 4.15: *Reactance of the LRC circuit at and near the resonance frequency.*

4.6 The Ionizer

4.6.1 Introduction

The geometry (shape and size) of the filament and its resistance play an import part in the ionization efficiency of the beam. The above factors need to be taken into consideration when designing a filament for the source. A schematic diagram showing the electrodes and potentials inside the ionizer is shown in figure 4.16. Optimization was done by:

- using a filament of a suitable resistance to increase the current of the electrons
- increasing the area of the filament
- designing a filament with a shape that will ionize the entire volume of the beam

These factors are discussed in detail in the following sections.

4.6.2 Ionization

The tantalum filament inside the ionizer is heated by a current of up to 20 A to emit electrons. Ionization is achieved by the collision of the electrons emitted in the filament with the atomic beam and then accelerated by an applied field. During the collision, filament electrons transfer energy to the atomic beam electrons, called the outermost bound electrons. If these outermost bound electrons gain enough energy to overcome the first ionization potential (13.6 eV), they escape the atom leaving a positive ion. There are two parameters that determine the ionization of a neutral atom:

1. temperature of the primary electrons (Te).
2. the electron density (N_e-).

Equation 4.5 [Bro65] shows the relationship between temperature and the mean energy of the primary electrons:

$$\overline{E} = \frac{3}{2} kT \qquad (4.5)$$

where:

k is Boltzmann's constant, and

T is the electron temperature in K.

The mean energy is directly proportional to the temperature of the particles. An increase in the temperature of the filament results in the emission of a large number of electrons (a high electron density, N_e-) that are accelerated to sufficient energy to ionize the neutral beam.

Electrons emitted from the filament are accelerated by an applied voltage of 1 kV, and the velocity of the electrons is calculated as follows:

$$E = \frac{1}{2}mv^2$$
$$v = \sqrt{\frac{2Ve}{m}} \qquad (4.6)$$
$$= 1.88 \times 10^7 m/s$$

Another factor that influences ionization is the time that the atoms spend in the ionization chamber, which is known as the ion confinement time (t_i) [Bro89]. The value of t_i is increased by decreasing the velocity of the hydrogen atoms, which takes place in the nozzle where the temperature of the beam is decreased. When the velocity of the neutral beam is decreased, the beam particles spend more time in the ionizer, which leads to more collisions with the primary electrons. The cylindrical shape of the ionizer has the advantage of confining electrons to the atomic beam volume, which increases the ionization.

4.6.3 Electrodes

The electrons emitted from the filament (G in figure 4.16) at a potential of typically ~1200 V leave the filament at different directions. They are then accelerated by the field produced by the electrode (E0 ~-2 kV), which is at a higher negative potential. Additional to that they are also accelerated by the voltage on the E1 electrode of ~ -1.8 kV. On the other side of the filament, electrons are repelled by the negative electrode E0 also at a potential of -2kV. Together E0 and E1 ensure that the electrons flow from the filament in the direction of the ionization chamber where ionization of the atoms occurs. The electrons then pass through E2 and E3. Due to the negative potential of E4, the electrons are reflected between E2 and E4 in the ionization chamber (E3). The beam enters the ionizer from E0 and proceed into the ionization chamber where it is ionized. The positive ions are attracted by the negative potential of E4, and move through E5 and E6 out of the ionizer. Electrodes E5 and E6 form an einzel lens that focuses the beam. The electrodes are isolated from each other by means of an isolator with a 30kV break down voltage.

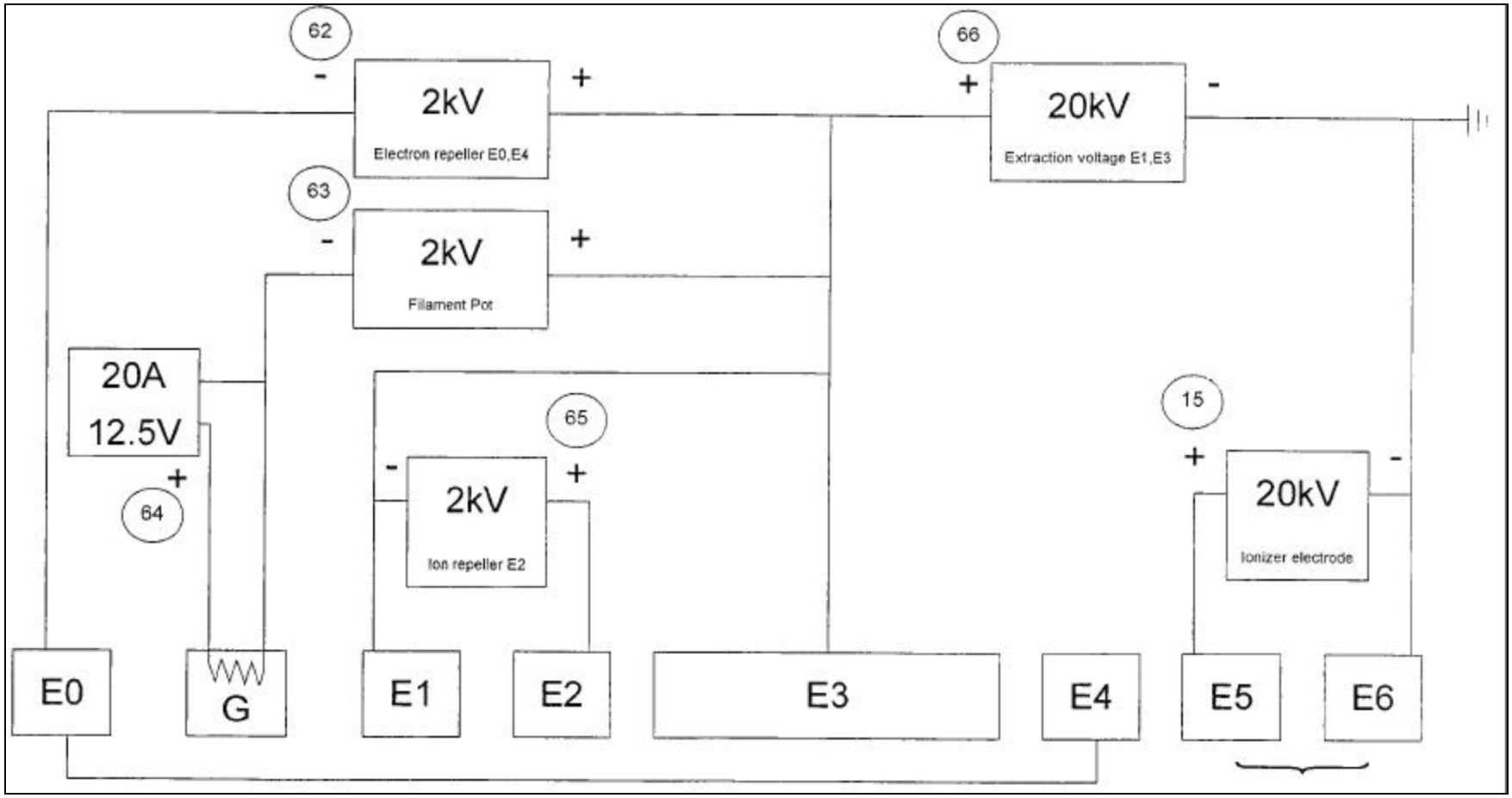

Figure 4.16: *Layout of the electrodes inside the ionizer. The filament is indicated by G.*

4.6.4 Results

Three filaments were investigated to determine the filament shape and size for optimum beam current. The results are depicted in the table below:

Table 4A: Results of experiments performed to investigate different filaments

	Filament1	**Filament2**	**Filament3**
Filament Type/material	***Ta***	***Ta***	***Ta***
Length (mm) **Thickness (mm)** **Width (mm)**	***27.7*** ***0.2*** ***1.2***	***51*** ***0.5*** ***1.2***	***55*** ***0.2*** ***1.2***
Resistance (@293K) (mW)	***17***	***22***	***27***
Max. Beam Intensity (mA)	***29***	***69***	**-**
Filament Current (A)	**19.97**	**16.40**	**-**
Area (m^2)	**$7.76x10^{-5}$**	**$1.73x10^{-4}$**	**$1.54x10^{-4}$**

The number of protons produced in the ionizer was calculated by dividing the beam current, measured with a Keithley ammeter by the electron charge:

$$p^+ = \textit{beam current/ electron charge.} \qquad (4.7)$$

The area of the filament is calculated using equation 4.8:

$$A = 2[(length \times width) + (length \times thickness)] \qquad (4.8)$$

Figure 4.17 shows the dependence of beam current on filament current.

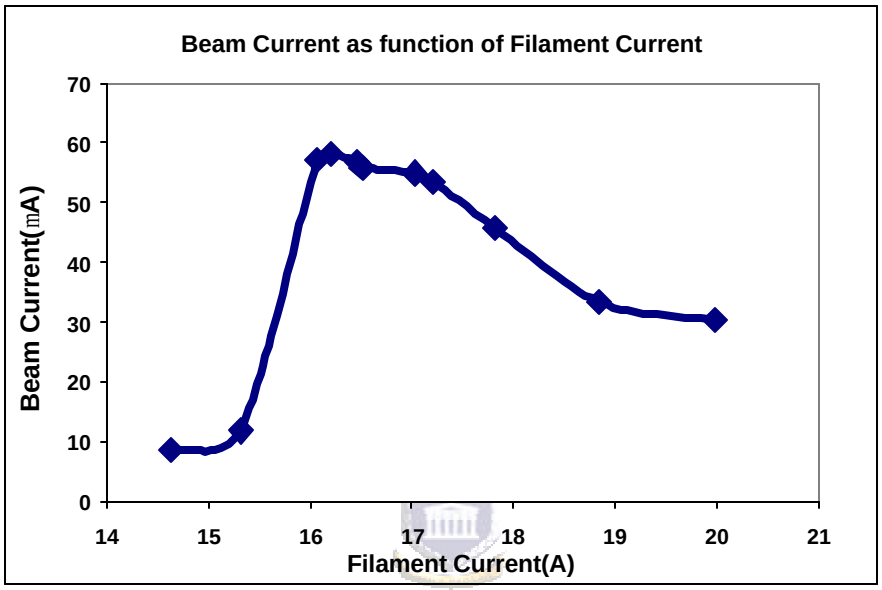

Figure 4.17: *Dependence of beam current on filament current for filament 2. The experiment was performed at 35 K using 203 divisions on the valve for the nitrogen gas.*

4.6.5 Efficiency of the Ionizer

The electron current density for both filaments when they are heated to the same temperature is calculated using equation (3.9):

$$j_e = 6.1\ A\ cm^{-2} \qquad (4.9)$$

The electron current density is a measure of the number of electrons that will gain enough energy to overcome the energy barrier (ionization potential) and escape the metal and become free electrons. The work function is the amount of energy that is

required to overcome this energy barrier for that type of material. Factors affecting the thermionic current are the temperature that the filament can withstand and the work function. The work function depends on the material that the filament is made from. The temperature is in turn affected by the evaporation rate and the lifetime of the filament [Ham71].

The number of electrons emitted is calculated using equation 4.10:

$$N_{e^-} = \frac{j_e \times A}{e^-} \qquad (4.10)$$

where:

j_e is the electron current density calculated in 4.9,

A is the area of the electron emitting filament,

e^- is the electron charge.

The number of electrons was calculated and is displayed in table 4B:

Table 4B: Electron current density for each filament

Filament	N_{e^-}
1	$2.98 \times 10^{15} e^-$ /sec
2	$6.60 \times 10^{15} e^-$ /sec
3	$5.87 \times 10^{15} e^-$ /sec

The number of protons produced during ionization using filament1 is: 1.81 x 10^{14} p^+/sec, and with filament2, 4.31 x 10^{14} p^+/sec **(**measured on the faraday cup). The pressure rise in the pressure tube was measured to be 9.6×10^{-5} mbar. This corresponds to 1.86×10^{16}

atoms per second by using the calibration function (see figure 4.6). The effectiveness of the ionizer is therefore:

$$\frac{4.3 \times 10^{14}}{1.86 \times 10^{16}} = 2.2\%$$

The expected beam current from each filament was calculated using equation 4.11 and the results are displayed in table 4C:

$$\text{Beam current} = A \times s \times N_p \times N_e \qquad (4.11)$$

where,

N_p is the number of particles for a hydrogen flow of 22 cm^3/min, which corresponds to 9.73×10^{18} atoms/sec,

N_e is the number of electrons emitted in the filament,

σ is the ionization cross section=0.1×10^{-16} cm^{-2}, and

A is area of the ionization column, with a diameter of 30 mm.

Table 4C: The calculated beam current for each filament

Filament	**Beam Current (mA)**
1	32
2	72.6
3	65

4.6.6 Discussion

For filament 2 only 17 A was used to heat the filament for maximum beam current while filament1 required maximum current available (19.8 A). Using lower currents is an advantage because at the maximum filament current (~19 to 20 A) produced excessive heat causing the filament electrodes to spark, resulting in beam loss. It is evident from the results that the maximum beam current can be obtained with filament2 without driving

the ionizer to its limits. A more stable beam is achievable with filament 2, because the chances of sparking are very low. Figure 4.17 shows the beam current as a function of filament current. The graph in figure 4.17 shows that the beam current reaches its maximum value at a value that does not coincide with the maximum filament current. At high currents, for example 19.98 A, the beam current is lower at a value of 30.30 μA, as compared to 58.22 μA at 16.21 A. Beam current decreases at high filament currents, between 18 A and 20 A. The reason is that the electrons on the walls of the ionizer are activated/ energized by the heat produced in the ionizer during the heating of the filament causing the electrons to collide with atoms in the beam. They do not have enough energy to ionize the beam, consequently the intensity of the beam is decreasing. The ability to produce high beam currents using low filament current is very important in ensuring less background.

Filament 3 (figure 4.20) has a higher resistance than the first two filaments. With this filament the beam current was expected to be 65μA. But, when experiments were performed, the results were very disappointing. The filament produced too many electrons causing a lot of heat in the ionizer. This then interfered with the vacuum and caused sparking in the ionizer. The filament current could not even be taken up to 15 A. Too much power was dissipated even at a low current resulting in no beam current at all. It also caused electrical discharge and a loss of vacuum. These results show that there is an optimum value for filament resistance; beyond this value optimum beam current cannot be achieved.

Another reason why filament 2 is the best candidate is that the number of electrons emitted by filament2 (electron density N_{e^-}) is much larger than the number of electrons emitted in filament1 and filament 3 (Table 4B). This is due to the fact that the number of electrons produced is directly proportional to the area of the emitting filament (equation 4.10), with filament 2 having a larger surface area than the other two filaments. This leads to higher ionization when using this filament, which increases the number of protons produced, thereby increasing the beam intensity.

The calculated values (in table 4C) and the measured values (in table 4A) of the beam current for the first two filaments are very close to each other. This shows that the methods used for optimizing the ion source were very effective.

Figure 4.18, 4.19 and 4.20 show pictures of the three filaments used in this study.

Figure 4.18: *Filament 1: 17 mW. The radius of the filament is 4.5 mm.*

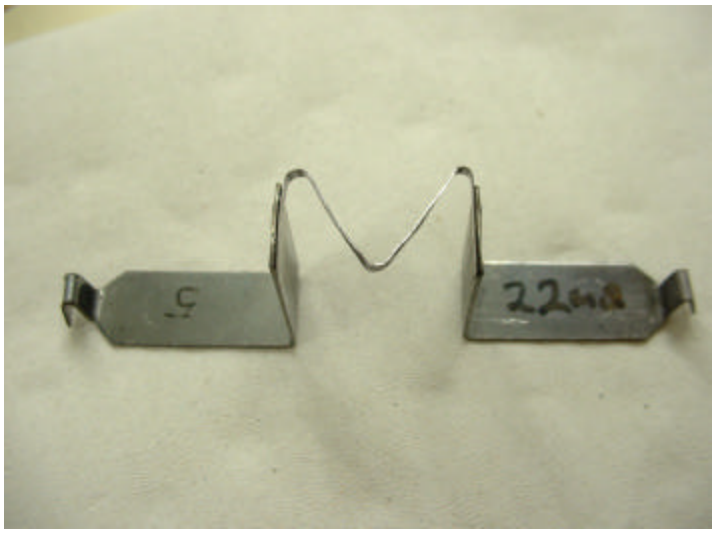

Figure 4.19*: The 22 mW filament (filament 2).*

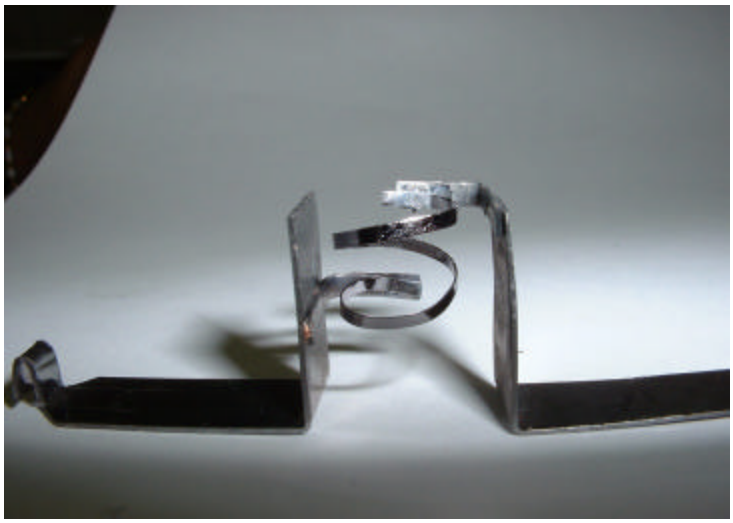

Figure 4.20: *Filament 3 (27 mW) with a spiral shape*

4.7 THE NOZZLE

4.7.1 Introduction

The beam emerging from the dissociator is now cooled in the nozzle and collimated by a 6 mm skimmer that is situated 14 mm from the converging nozzle made from copper. The skimmer is housed in a separate vacuum chamber at a lower pressure. Before May 1997 all the nozzles used at iThemba LABS were made from sapphire. They were then changed to aluminum due to small crack that developed in the sapphire. Aluminum was chosen because of its low cost and it is easily accessible.

4.7.2 Results

During this study three nozzles were tested, one is made of aluminum and two are made from copper. The results are displayed in Table 4D.

Table 4D: Results of experiments performed to investigate different nozzle types

	Nozzle 1	Nozzle 2	Nozzle 3
Material Type	***Al***	***Cu***	***Cu***
Inner diameter (mm)	***6.5***	***7.5***	***11.5***
Exit diameter (mm)	***3***	***3***	***3***
Max beam current (mA)	***29***	***58.22***	***69***

Calculations:

The area of the nozzle at the throat/exit is 7.069×10^{-3} m^2.

Figure 4.21 illustrates the relationship between the inner diameter of the nozzle and the beam intensity.

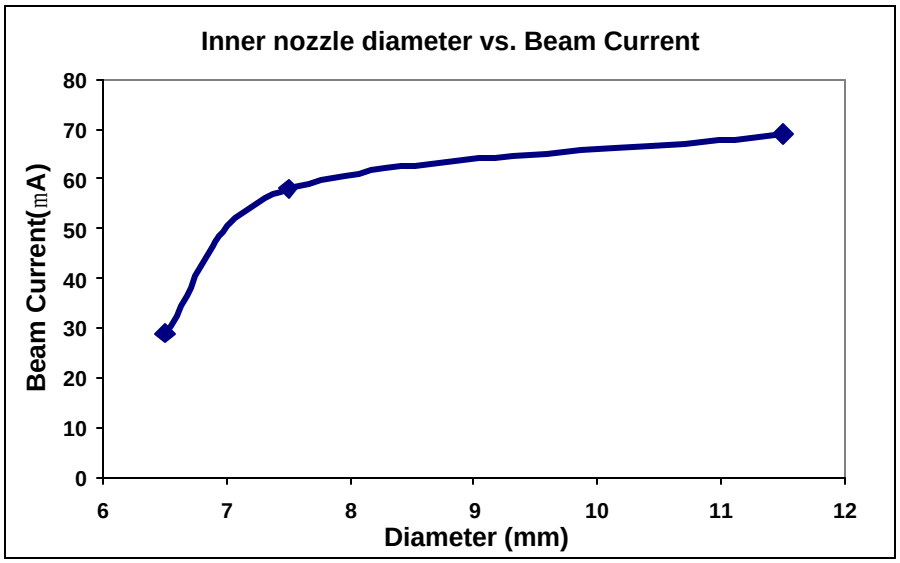

Figure 4.21: *The dependence of beam current on the inner diameter of the nozzle.*

4.7.3 Discussion

It was found that the bigger the difference between the inner and the exit diameter, the higher the beam current. Results illustrate that the beam expands more as the difference between the inner and the exit diameter increases. The copper nozzle produces better results than the aluminum. This is due to the fact that the copper was treated with H_2PO_4 and HF to remove all the impurities. The copper nozzle was smoother and cleaner than the Al nozzle.

The pressure at the throat/exit of the nozzle (3 mm in diamenter) is large when compared to the pressure at the entrance of the nozzle (20 mm in diameter) and the 11.5 mm inner diameter area. The large pressure gradient results in the expansion of the beam. Nozzle 3 has a bigger volume than of first two nozzles. The bigger volume will allow for a bigger flow of atoms and an increased pressure gradient. This then ensures that the beam expands when it exits the 3 mm throat.

CHAPTER 5

NUCLEAR POLARIZATION

5.1 Jachard Method

5.1.1 Introduction

The Jachard method is used to measure polarization before the beam is injected into SPC2. This method is used to determine the strong/ weak magnetic field settings for optimum polarization. The measurement is based on the fact that the ionization cross-section for polarized atoms $\sigma\uparrow$ is larger that the cross-section for the unpolarized atoms $\sigma\uparrow\downarrow$ ($\sigma\uparrow > \sigma\uparrow\downarrow$). Beam current measured for atoms in a polarized state is higher. By switching the nuclear polarizing on and off at a rate of 15 Hz and measuring the beam current on a spectrum analyzer the effect of nuclear polarization will be measured.

5.1.2 Procedure

1. The first step is to decrease the filament current to ~ 10μA.
2. The pulse generator (FG 800) is then connected to the 500 Hz spectrum analyzer.
3. A spectrum is taken for each setting of the current through the coils of the magnet in the strong and weak field units.

The steps for the strong field and weak field settings are listed in Appendix A.

5.1.3 Results

Figures 5.1 and 5.2 show the results of the Jachard measurements. Figure 5.1 shows the results of the weak field measurements and figure 5.2 shows the results of the strong

field measurements. The values of the current through the coils required for the measurements in SPC2 can be read-off from the graph.

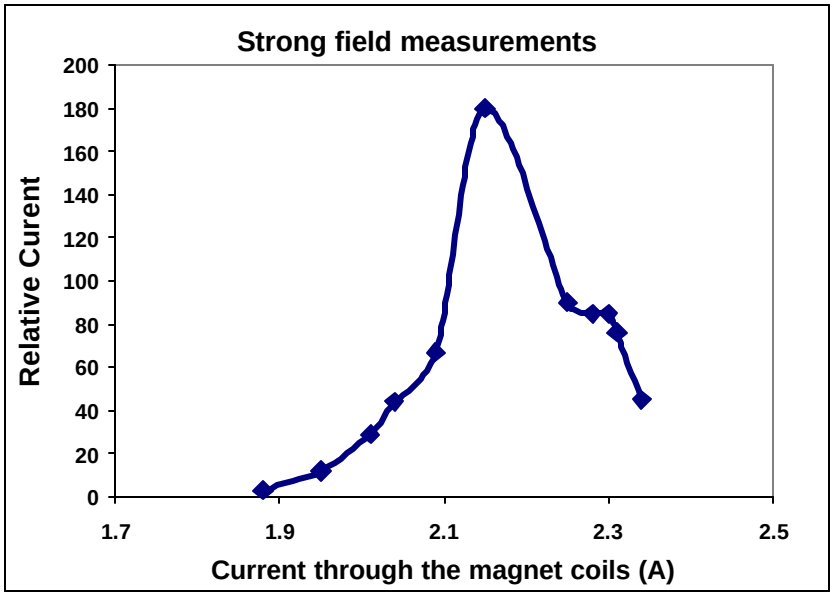

Figure 5.1: *Results of the strong field measurements.*

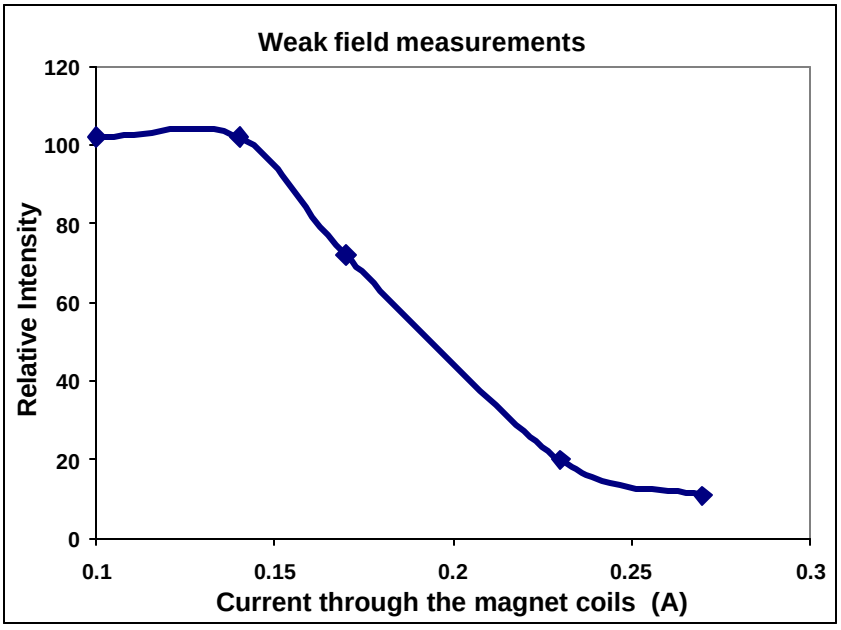

Figure 5.2: *Results of the weak field measurements.*

5.2 Beam depolarization due to the beam lines

Figure 5.3shows the beam lines between the ion source and SPC2. The line consist of eight solenoids and two 45° bending magnets. The Wien filter is used to produce an additional shift of 18.6° in the direction of polarization without deflecting the beam. When injected into the SPC2 the average polarization vector will be vertical aligned with a total average precession of 270° (see Appendix B). Due to the big emmitance, parts the beam experiences different magnetic fields and therefore proceeds with different directions with a resultant spread in polarization. The emmitance cannot be decreased but the spread in polarization can be made small by tuning the beam line elements. The following equation describe the spin motion S in a magnetic field:

$$\frac{ds}{dt} = S \times w_s \qquad (5.8)$$

with the:

$$w_s = \frac{e}{m}(1+a)B \qquad (5.9)$$

where:

w_s is the axial precession vector,

B is the magnetic field, and

a is the gyromagnetic anomaly (1.7928) for protons.

In the same manner the particle motion for the change in linear momentum, p, is described by the Lorentz equation:

$$\frac{dp}{dt} = p \times w_p \qquad (5.10)$$

$$w_p = \frac{eB}{m_0 g} \qquad (5.11)$$

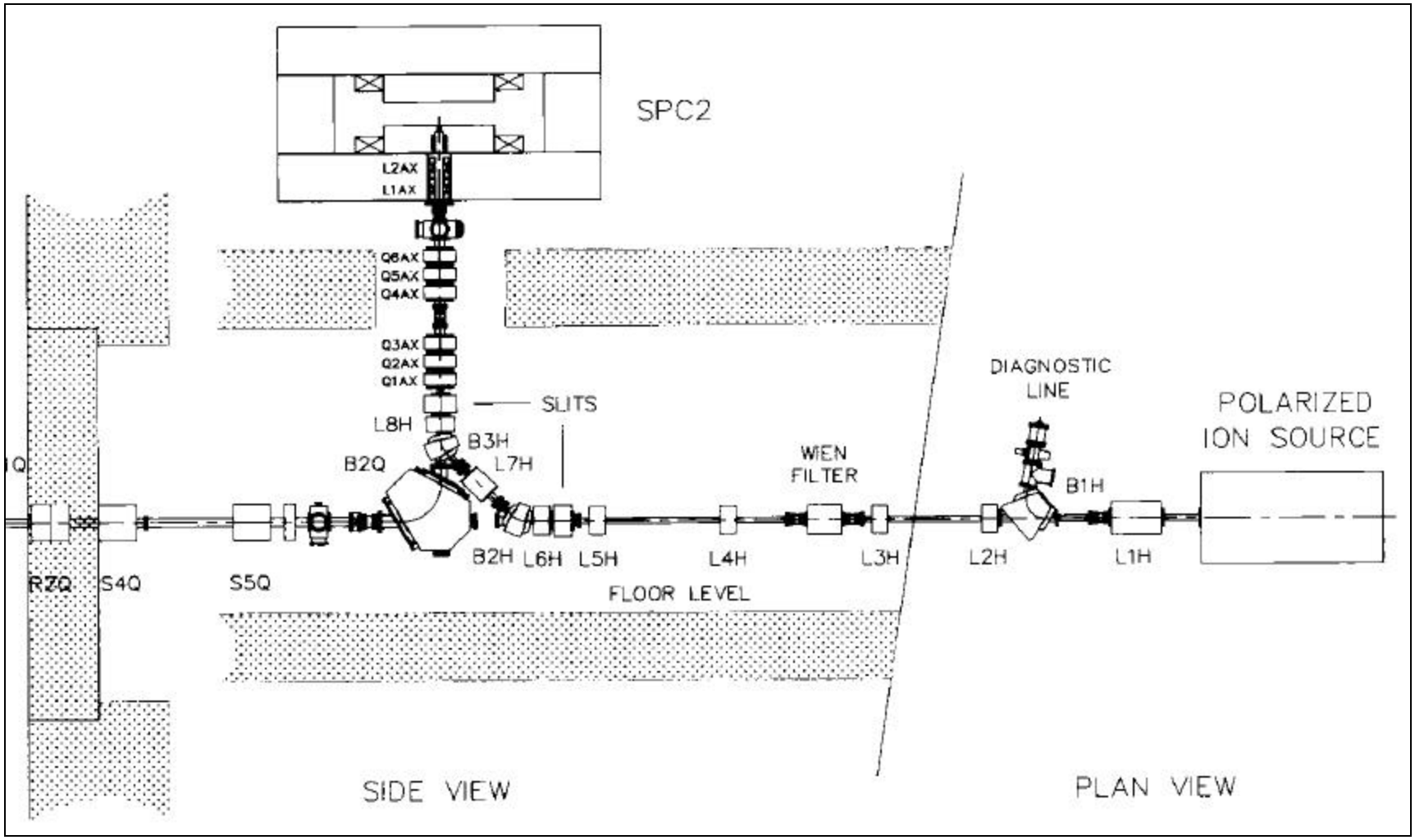

Figure 5.3: *The beam line between the ion source for polarized protons and SPC2*

Calculations were done [Cro98] using these equations as well as equations that describe the field distribution of the solenoids fields and distribution of the bending magnets above the median plane. These calculations showed that depolarization is negligible inside SPC2 and in the beam lines consisting of dipoles and quadrupoles but not in the solenoids. It was shown that the beam should be small as possible when passing through the solenoids. It was also shown that solenoid pairs should be tuned to have equal magnetic fields to obtain symmetrical beam envelopes as shown in figure 5.4. Changing the fields of the solenoids early in the beamline has larger depolarization effects.

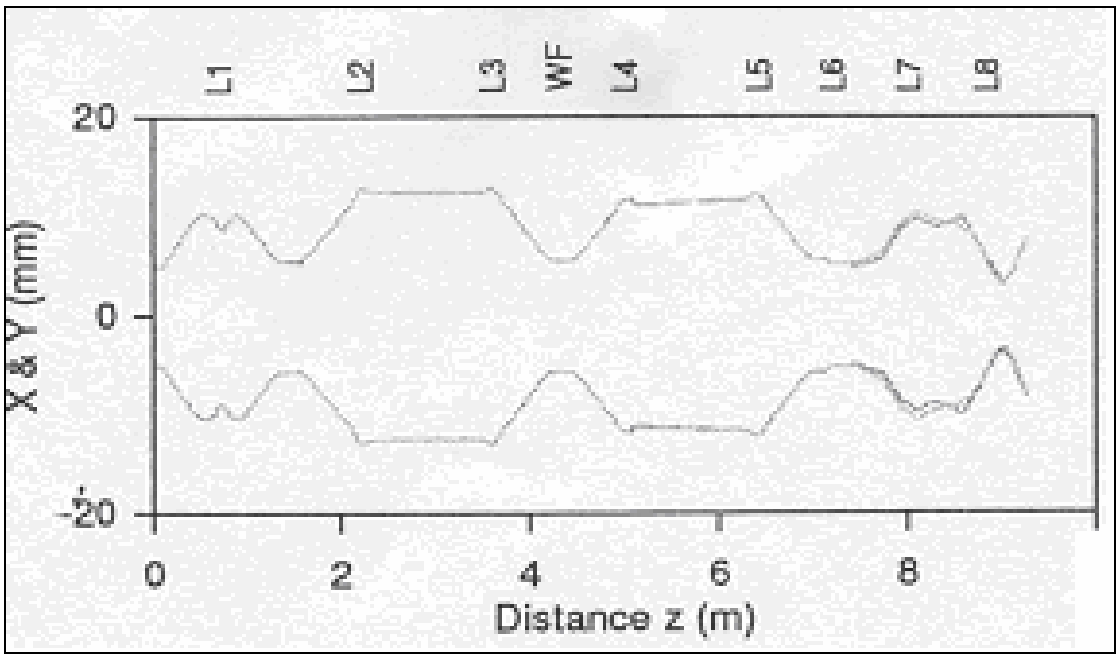

Figure 5.4: *Symmetrical beam envelope of a polarized proton beam in the H-line.*

CHAPTER 6

CONCLUSIONS

Proper operation and maintenance of the ion source ensures that a stable beam of polarized protons is generated when required. Results from previous chapters proved that with the correct combination of nozzle temperature and nitrogen gas, nozzle diameter, filament type and potential a high beam intensity can easily be produced.

Results showed that when a high beam current is required a combination of the following is required:

- High gas flow (hydrogen gas) and a high RF power in the dissociator,
  - A flow of between 22 and 24 cm^3/min of hydrogen gas with a RF power of 100 to 150 W produces a high dissociation degree, which results in a higher beam current.
- Although the flow of hydrogen gas is important for high beam currents, this causes an increase in the pressure in the chambers. This is contra-productive for good beam transmission. Pumps with nominal pumping speeds of more than 1500 ls^{-1} are needed to produce a pressure of less than 1×10^{-7} mbar inside the ionization chamber. Preference should be given to turbo pumps with a high pumping speed of more than 1200 l /s for hydrogen.
- The beam temperature has to be decreased to about 27 or 28 K and a bigger supply of nitrogen gas must be used.
- A copper nozzle with a diameter of 11.5 mm. For best results the nozzle has to be treated with HF and H_2PO_4,
- A tantalum filament with a resistance of 22 mΩ with a shape that can ionize over the entire atomic beam volume. From the results it was deduced that the triangular-shaped filament produces the best results,
- A filament current that can heat the filament up to the optimum temperature of thermionic emission.

Optimum resistance for a filament should produce a high beam current without using maximum filaments currents, therefore generates a more stable beam. This filament only requires a current of ~17 A to heat up to the desired temperature. The 11.5 mm nozzle produces a large pressure gradient that expands the beam when it exits the nozzle. The above combination yields the best results and stable beam currents of approximately 69 μA.

Another important factor during the operation of the ion source is maintenance. The Pyrex tube has to be cleaned with alcohol after every third or fourth operation to remove the sputtered of metal on the glass surface [Dic65]. When it is dirty, the beam current decreases, after cleaning it the beam current goes back to its normal value. The nozzle also has to be cleaned with alcohol and a clean, dry, soft paper to remove the SiO_2 that deposits on its walls. When the ion source is not in use, the dissociator power supply has to be switched off but its water supply (for cooling) has to be on. It is also an advantage to let dry nitrogen gas into the ion source before venting the ion source. This is done so that the nitrogen gas sticks to the walls of the source before air and moisture enters the source. This decreases the pump-down time because the pumping speed for nitrogen is 20-25 % higher than for hydrogen.

The beam current can also be increased by [Dic65]:

- Putting 10% of water vapour into the hydrogen to improve dissociation. It was found that this could increase the dissociation degree by 100%.
- Filling the Pyrex tube briefly with 30% diluted hydrofluoric acid and rinsing with distilled water removes rough spots on the glass surface.
- The efficiency of the ionizer can be increased by applying a magnetic field of several hundred Gauss.

Another useful method is to determine the values of the strong and the weak fields in the ion source, using the Jachard method, before lengthy and time-consuming efforts are done in the beam lines.

APPENDIX A

Strong field Measurements

3. Disconnect "SF-PLS" cable from the electronic cabinet (left, top, second rack) and connect it to the pulse generator FG800 (T-piece). The end of this cable is connected to the strong field RF generator (1000-2000 MHz, MOD 6051) (marked 80) external pulse connector.
4. Turn MODULATION knob on unit marked 80 to "pulse".
5. Turn the frequency of this generator to 1448 MHz by observing the reading on the meter called "FREKWENSIEMETER".
6. Turn the knob on the spectrum analyzer so that the marker is at 15 MHz.
7. Turn the strong field power supply NTN 35 M-6,5 (marked 80) to values ranging from -1-82 A by 0.02 A steps very slowly and watch the marker.
8. At a certain time the marker will be at the top of a pulse on the oscillator.
9. By changing the field (power supply settings) the marker can be optimized to be raised higher. This field value will then be the optimum value for strong field polarization.

Weak field Measurements

10. Do the same with the weak field, using cable "WF PLS" and power supply NTN 3.6-6.5 marked S1.

Finally

11. Put cables SF-PLS and WF-PLS back on the connections at the left top of the cabinet.
12. Switch this apparatus to "aan" and set the time to 15 seconds. The beam is now ready for measuring polarization.
13. Set the Wien filter.

APPENDIX B

The average spin procession in the two 45^0 bending magnets is 251.4^0 as can be calculated from the following equations. If I is the angular momentum, then

$$\frac{dI}{dt} = \frac{g m_0}{\hbar} BI$$

with,
g the gyromanetic ratio =-3×10^{-3},
m_0 is the Bohr magneton,
h is Plancks' constant, and
B is the magnetic field.

The solution for this differential equation is:

$$I = Ie^{\frac{gm_0}{\hbar}Bt} = Ie^{a_I t}$$

The equation for the linear momentum for the proton motion is:

$$\frac{dp}{dt} = p \times w_p \text{ (see equation 5.10)}$$

The solution for these differential equation is:

$$p = pe^{\frac{qB_0}{m}t} = pe^{a_p t}$$

If the proton momentum changes direction with an angle of $a_p t$ the spin momentum will change with an angle of $a_I t$, the relation between these two angles is:

$$\frac{a_I}{a_p} = \frac{g m_0 m 2p}{hq}$$

if a_p is 90^0 the value of a_I is 251^0.

APPENDIX C

Constants

	Quantity	***Symbol***	***Value*** ***SI Unit***
1	*Elementary charge*	*e*	*1.602 E -19 C*
2	*Electron mass*	m_e	*9.109 E- 31 kg*
3	*Proton mass*	m_p	*1.673 E-27 kg*
4	*Neutron mass*	m_n	*1.675 E-27 kg*
5	*Bohr magneton*	m_e	*9.274 E-24 $J.T^{-1}$*
6	*Boltzman constant*	$k= R/N_A$	*1.381 E-23 $J.K^{-1}$*
7	*Stephan- Boltzman constant*	*s*	*5.670 E-8 $W.m^{-2}.K^{-4}$*
8	*Planck constant*	*h* *?= h/2p*	*6.626 E-34 J.s* *1.054 E-34 J.s*
9	*Molar gas constant*	*R*	*8.314 $J.mol^{-1}.K^{-1}$* *287 $J.kg^{-1}.K^{-1}$*
10	Emissivity of Tantalum	*e*	0.26
12	*Specific heat ration for air*	*g*	*1.4*
13	*Richardson Constant*	**R**	*120 A $cm^{-2} K^{-2}$*
14	*Work function of Ta*	*W*	*4.12*

Energy Equivalents

	Quantity	***Symbol***	***Value***
1	*Electron Volt*	*eV*	*1.602 E-19 J*
2	*Electron mass*	m_e	*0.511 MeV*
3	*Proton mass*	m_p	*938.272 MeV*
4	*Planck constant*	*?*	*6.582 E –22 MeV*

Definitions

Isentropic flow: Flow that is frictionless and adiabatic with no discontinuities in the flow properties. This flow is valid for nozzles where the changing of the area is the predominant cause of the changed flow conditions [Hug76].

Sonic flow: Flow whereby the velocity of the particles is equal to the local speed of sound. This is when the Mach number is equal to 1 [Gha05].

Supersonic flow: Mach number is greater than 1, the velocity of the particles is greater than the speed of sound.

Subsonic flow: The velocity of the particles is less than the speed of sound, i.e. Mach number is less than 1, the beam will not expand when it exits the nozzle.

Critical conditions: The flow is sonic [Gha05].

Shock wave: Region of discontinuity in the flow (nonisentropic region). There is a large density, pressure, temperature and velocity gradient in this region [Mil88].

Polarization Statistics

Energy (MeV)	Strong Field (A)	Weak Field (A)	Polarization Strong Field (%) p-down	Polarization Weak Field (%) p-up	Polarization (%)
100	2.47	0.05	86	80	83
	2.41	0.05	85.7	79	82.6
	2.41	0.05	84.9	73.7	79.8
	2.29	0	70	81	75.8
	-1.72	0.14	76	85.7	81.2
	-2.16	0.15	71	76	73
	-2.14	0.29	73.9	79.6	76.9
130	-1.37	0.15	64	84	76
	-1.76	0.14	72.6	87.4	80.2
	-2.2	0.16	74	85	79.9
	-2.15	-0.09	74	83.5	79.2
160	-2.1	0.12	71	81	76

Energy (MeV)	Strong Field (A)	Weak Field (A)	Polarization Strong Field (%) p-down	Polarization Weak Field (%) p-up	Polarization (%)
	-1.38	**-0.15**	**75**	**88**	**81**
200	**-1.35**	**0.11**	**70**	**77**	**73**
	-1.60	**0.11**	**73**	**87**	**80**
	-1.65	**0.10**	**78**	**81**	**80**
	-1.65	**0.10**	**74**	**77**	**75**

REFERENCES

[Bim98] Bimbot R., From the Discovery of Radioactivity to the Production of Radioactive Beams, Cyclotrons and their Applications 1998 (ed. Baron E & Lieuvin M), Proceedings of the 15th International Conference, Caen, France.

[Bro89] Brown I. G., The Plasma Physics of Ion Sources, The Physics and Technology of Ion Sources, A Wiley- Interscience Publication, John Wiley & Sons, New York (1989). p. 8-9,17-21.

[Bro95] Brown I., Fundamental Processes, Handbook of Ion Sources (ed. Wolf B), CRC Press 1995, p.11, 28-29.

[Bur63] Burcham W.E., Nuclear Physics, An Introduction, William Clowes and Sons (1963), p. 618.

[Con92] Conradie J. L., Improved Proton Beam Quality and Intensity from a 200 MeV Cyclotron System, *Dissertation presented for the degree of Doctor of Philosophy in Physics at the University of Stellenbosch (1992).*

[Cro98] Cronje P.M., Beam depolarization in the NAC Beamlines and Cyclotrons, Cyclotrons and their applications 98, Caen, June 1998.

[Dic65] Dickson J. M., Polarized Ion Sources and the Acceleration of Polarized Beams, Progress in Nuclear Techniques and Instrumentation, Volume1 (ed. Farley F.J.M), North-Holland Publishing Company-Amsterdam.
p. 114,138-139,151-154.

[Dou85] Douglas J. F, Gasiorek J.M & Suraffield J.A. Fluid Mechanics, Second Edition, John Wiley & Sons, New York, 1985, p.411, 406.

[Gla68] Glavish H.F., A Strong Field Ionizer for an Atomic Beam Polarized Ion Source, Nuclear Instruments And Methods, (ed. F.J.M Farley), North-Holland Publishing Co., (1968) p. 1.

[Gha05] Ghajar A. J., Compressible Flow, The Engineering Handbook Richard Second Edition (ed. Dorf R.C), CRC Press (2005).

[Ham71] Hamilton G. W., Ion Source Technology, Proceedings of the Symposium on Ion Source and Formation of Ion Beams (ed. Sluyters M.J.), 19-21 October 1971, Brookhaven National Laboratory, Upton, New York.

[Mai02] Maine P.M., Design and Optimization of New beamlines for iThemba Laboratory for Accelerator Based Sciences (iThemba LABS), MSc Thesis, Center for Applied Radiation Science and Technology, University of North West, 2002.

[Mil88] Miller D. R., Free Jet Sources, Atomic and Molecular Beam Methods, Volume 1(ed. Giacinto Scoles), Oxford University Press, 1988.

[Nac76] National Accelerator Center, Technical Report of the Accelerator Task Group (National Accelerator Projector), 1976.

[Nac88] National Accelerator Center, Annual Report, June 1988.

[Nas03] Nass A. et al., The HERMES polarized atomic beam source, Nuclear Instruments and Methods in Physics Research, Section A (2003), p.634-635. *Available online at www.sciencedirect.com*

REFERENCEs

[WWW1] http://www4.tlabs.ac.za/vanrooyeen

[WWW2] http://iris.riken.go.jp/pis/dissociator.html

[Ros92] Rossbach J & Schumüser P, CERN Accelerator School, University of Jyväskylä, Finland, 7-18 September 1992, p.29.

[Yar60] Yarwood J., Atomic Physics, University Tutorial Press (1960), p102.

[Hug76] Hughs W.F. & Brighton J.A., Shaum's Outline Series 1976, p138.